Ph.D. Dissertation of Energy System Engineering

Development of ZIF-activated carbon membrane for H_2/CO_2 and CH_4/CO_2 separation

H_2/CO_2 및 CH_4/CO_2 분리용 ZIF 활성탄막 개발

2022 August

Graduate School of Energy System Engineering

Seoul National University

Muhammad Amin

Development of ZIF−activated carbon membrane for H_2/CO_2 and CH_4/CO_2 separation

Eunhyea Chung

Submitting a Ph.D. Dissertation of

Energy System Engineering

2022 August

Seoul National University

Energy System Engineering

Muhammad Amin

Chair _____(Seal)

Vice Chair _____(Seal)

Examiner _____(Seal)

Examiner _____(Seal)

Examiner _____(Seal)

Table of Contents

List of Figures

List of Tables

Abstract

In this thesis, the zeolitic imidazolate framework (ZIF) membrane was developed with the incorporation of activated carbon (AC) and aluminosilicate (AS). For the preparation of AC, H_3PO_4 was used as an activator agent to create an abundant pore structure. The Brunauer-Emmett-Teller (BET) surface area of AC derived from algae was 783.53 m^2/g. The X-ray diffraction (XRD) analysis of AS revealed that AS were crystalline in structure. The surface characteristics of the modified membrane were observed by using XRD and scanning electron microscopy (SEM) analysis.

The produced membrane exhibited both particle homogeneous distribution and efficient adhesion. Single gas (H_2, CH_4, and CO_2) tests were performed at room temperature and 100°C. The two mixtures of gases, H_2/CO_2 and CH_4/CO_2, were tested at room temperature and 100°C. Permeation results from the ZIF membrane revealed the permeation value of H_2 and CO_2 were 3164.17 and 156.11 (Barrer), respectively, at room temperature. Permeation results from the ZIF-AC-AS membrane revealed the permeation value of CH_4 and CO_2 were 207.46 and 232.23 (Barrer), respectively, at room temperature. As the temperature rises from room temperature to 100 °C, the permeation values of CH_4 and CO_2 decreased slightly to 146.89 and 203.58 (Barrer), respectively.

The author of this thesis is a Global Korea Scholarship scholar sponsored by the Korean Government.

Keywords: zeolitic imidazolate framework, Activated Carbon, Aluminosilicate, Membrane

Student Number: 2019-37498

Chapter 1. Introduction

1.1 Background

The term “coal” is a carbonaceous substance formed from the remains of vegetation by partial decomposition [1]. The quality of coal is divided into 4 types: low to high rank peat, lignite, bituminous, and anthracite. Anthracite has the highest carbon content of any coal and it is considered a good quality of coal among all types of coal.

Coal gasification is the process that converts carbonaceous materials into useful products like carbon dioxide, carbon monoxide, hydrogen, methane, etc. In coal gasification, the main process is considered the reaction of the carbon in coal with steam [2]. Coal gasification is carried out through fluidized bed gasification, fixed bed gasification, moving bed gasification, entrained flow gasification, or plasma gasification processes. Among all these gasification processes, entrained flow and plasma gasification are carried out from 1200 ºC to 1700 °C. The remaining gasification processes are carried out at below 1200 °C. The product gas composition depends upon the quality of coal and the type of gasifier [3]. Figure 1 illustrates the schematic diagram of the coal gasification process [4].

Many coal reserves contain a minor amount of sulfur so H_2S is formed during the coal gasification process [5]. Some of the additional product gases such as benzene, toluene, tar, hydrocarbons, and phenols are also formed as a byproduct due to the various components of coal [2]. Table 1 shows the typical gas compositions from the coal gasification process.

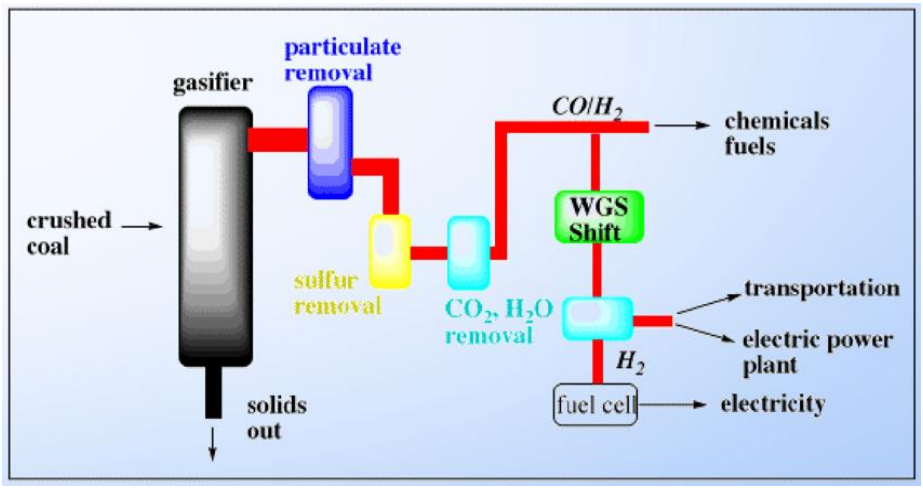

Figure 1. Schematic diagram of coal gasification [4].

Table 1. Coal gasification gases composition [6] [7]

Gases (Units)	**Composition** [6]	**Composition** [7]
H_2 (%dry)	44	38
CO (%dry)	28	45
CO_2 (%dry)	18	15
H_2O (%Wet)	16	---
CH_4 (%dry)	10	250 ppm
C_6H_6 (g/Nm^3 dry)	4.11	---
C_7H_8 (g/Nm^3 dry)	0.68	---
$C_{10}H_8$ (g/Nm^3 dry)	0.68	---
H_2S	---	0.9
N_2	---	2

For the separation and purification of these product gases (H_2, CO_2, CO, CH_4, C_6H_6, C_7H_8, H_2S, etc.), the application of separation technologies is required. Commonly used technologies for the purification and separation of gases are membrane technologies, pressure swing adsorption [8], cryogenic distillation [9], and metal hydride separation [8].

A membrane is a semipermeable layered separator that separates gases by acting as a selective mass transport barrier. Gas separation by membrane technology is a well-known approach in the industrial world because of its low capital and operational expenses, continuous process, and small footprint. Membranes are classified into metallic (porous and dense), inorganic (oxides, zeolites, glasses, ceramics), and carbon and polymer [10]. Figure 2 shows the schematic diagram of the membrane process.

Another separation technique is pressure swing adsorption (PSA). It is a relatively well-established process in the industry because no heating is needed for regeneration which causes the low capital cost. PSA is most commonly used for the purification of CH_4, H_2, CO, and CO_2. Different types of adsorbents such as molecular sieve, zeolite, silica gel, activated alumina, and AC and are used as an adsorbent for the PSA process. Nowadays, scientists reveal that slight adjustment in these existing adsorbents results in better purification and separation efficiency [8]. The adsorbent is considered a key for high separation performance. The most commonly used adsorbents are zeolites and AC [11]. The physicochemical properties of AC can be systematically adjusted by varying pyrolysis conditions. The heavy components such as CO_2 gas are captured in a porous medium, and the light components such as CH_4 bypass the column and are recovered downstream at higher purity. The most important factors that maximize the light gas purity are adsorption pressure, adsorption time, and adsorbate superficial velocity. Figure 3 shows the schematic process description of PSA [12].

Another separation technology is distillation, also known as cryogenic separation. The distillation process operates at a low temperature and is used to liquefy and purify gases from gas mixtures [9]. The basic principle of cryogenic distillation is to separate and purify the gas by utilizing the difference in the relative volatility of different components in the feed gas [8]. The cryogenic gas purification and separation method comprises fractional condensation and distillation of the gas at low temperatures. Commercially, low-temperature distillation, also known as cryogenic separation, is used to liquefy and purify CO_2 from high-purity sources [13]. Figure 4 shows the schematic process description of the cryogenic process [14].

Another separation technology uses metal hydride. The metal hydride purifies gases using gas storage alloys to absorb and desorb the gas reversibly. The most commonly used alloys for hydrogen storage are zirconium, titanium, magnesium, and rare earth alloys [8]. The $LaNi_5$-type alloys are used for hydrogen purification because these types of alloys exhibit good cyclic stability. In metal hydrides, two purification techniques can be implemented: running flow (batch operation) and flow-through (continuous operation). Process performance can be improved by adjusting the ratio between the inlet and outlet gas streams. To achieve a high hydrogen recovery rate and high energy efficiency, efficient heat transport is required to maintain isothermal temperatures across the metal hydride bed [15]. Figure 5 shows the schematic process description of the metal hydride separations [16].

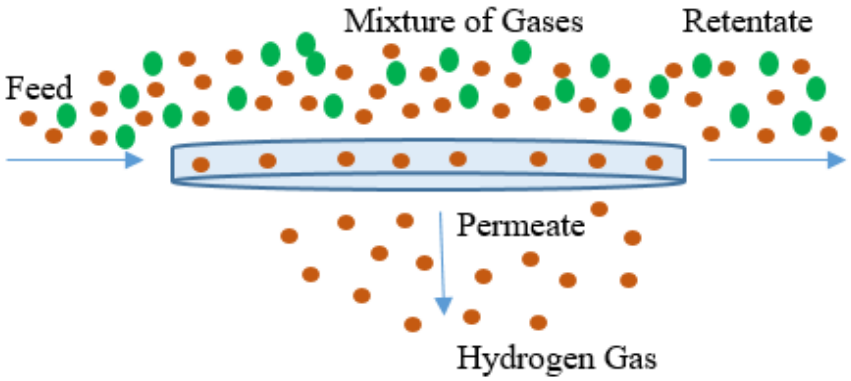

Figure 2. Schematic diagram of membrane separation [17]

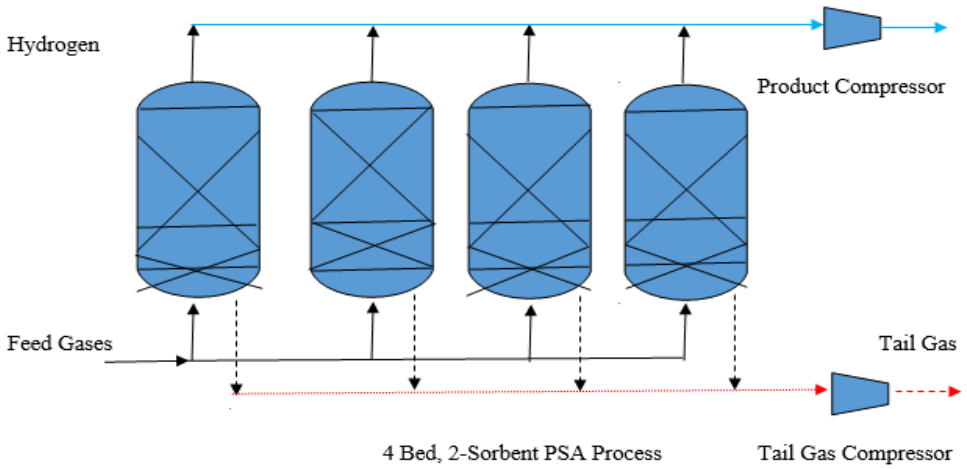

Figure 3. Schematic diagram of pressure swing adsorption for gases separation [12]

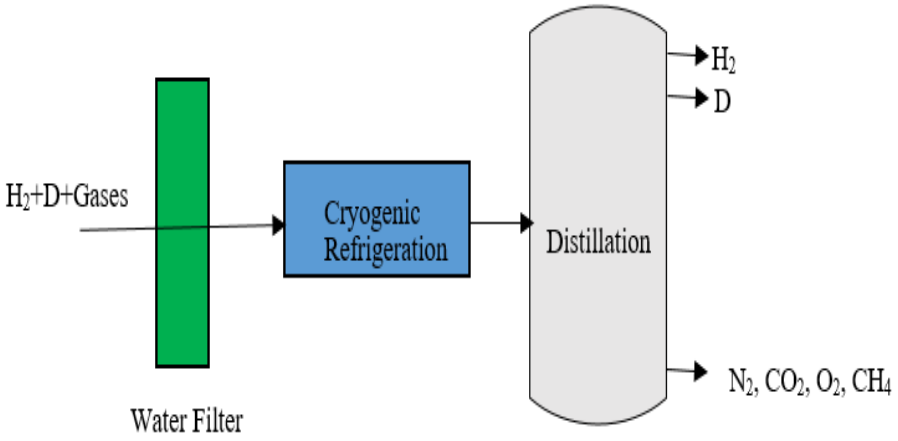

Figure 4. Schematic diagram of cryogenic separation [14]

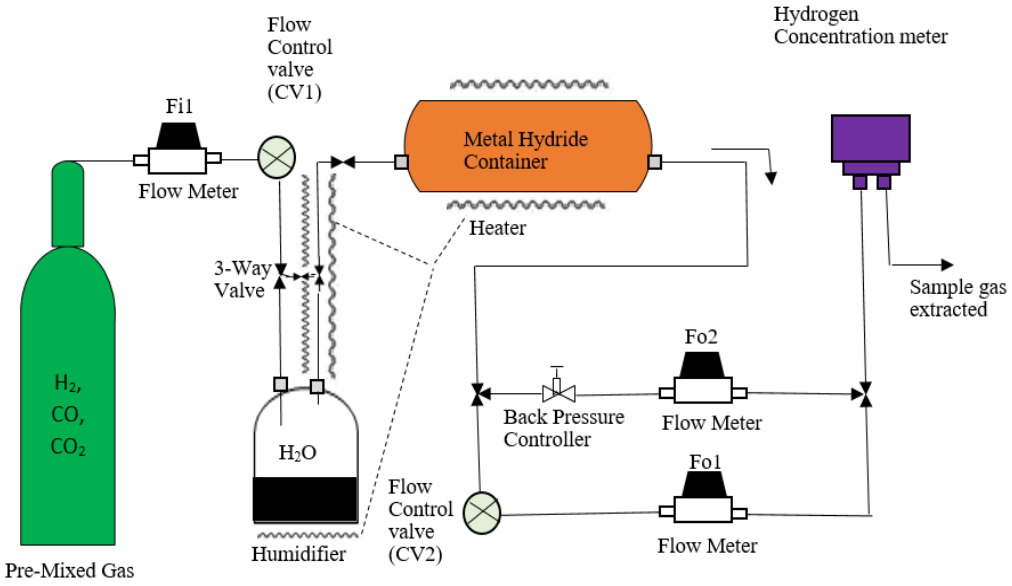

Figure 5. Schematic diagram of metal hydrides for gases separation [16]

The gas separation or purification processes are expensive because they generally require successful operation of a series of distillation columns or membrane systems [18]. These systems also make the processes more complicated. The total cost of the purification process might be decreased by combining more than two distinct separation technologies into a single system, which can be referred to as a hybrid system. One of the hybrid system is a membrane system in conjunction with another unit activity or any other chemical process that consists of a single unit operation. The hybrid technologies will make the gas separation process less expensive and enhance the gas separation efficiency [19]. The example of a hybrid system (distillation-membrane pilot plant) for gas separation is shown in Figure 6. The gas mixture that has been made in the column of cryogenic distillation would be sent to the membrane system where an aqueous solution extract the target gas [19].

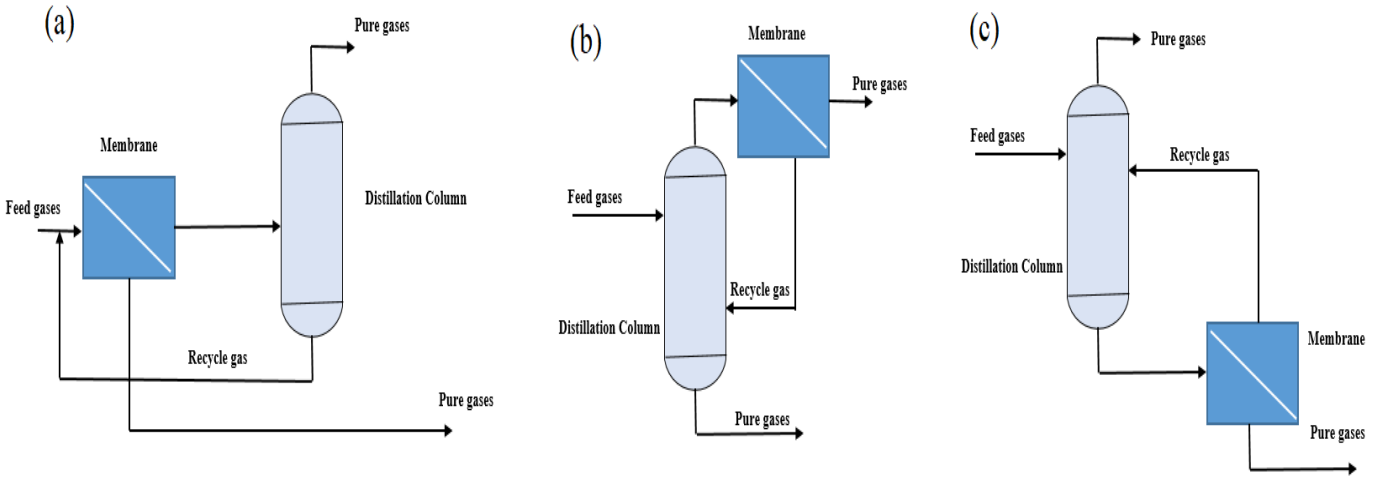

Figure 6. Hybrid system for gases separation [19]

Due to the importance of hybrid systems, this study tried to develop a membrane that could be in conjunction with the other existing industrial hybrid system.

As described previously, a membrane is a semi-permeable layer or separator that separates gases by acting as a selective mass transport barrier. The transport coefficients are defined in two ways: permeability and permeance. In addition, the composition of the gas mixture must be considered when determining the best separation procedure [20]. The gas separation is feasible via a pressure-driven process using membrane technology but the properties of the membrane are dependent on numerous aspects such as the material, thickness, structure, membrane configuration, and module system design [21]. For higher permeability, a smaller membrane area is advantageous. The separation process is considered more efficient at higher selectivity. Increasing the feed pressure in the membrane separation process leads to higher flux. Changes in feed pressure and gas composition can affect the adsorption characteristics of gas molecules in the membrane. Knudsen diffusion, surface diffusion, and molecular sieving are the three processes in the gas transport mechanism through the membrane [22]. The adsorption characteristics and the difference in the kinetic diameters of the gas molecules determine the transport mechanism in the membrane.

Membranes are generally utilized in industrial-scale separation operations at a variety of temperatures, feed compositions, feed pressures, and with sweep gas on the permeate side. Selectivity and permeability are the most significant properties of a membrane. A variety of membranes are useful in separating industrial gases into a variety of valuable products. Most commonly, membranes are classified as organic (polymer), inorganic (zeolite), metallic, metallic alloys, ceramic oxides, and carbon molecular sieves). Figure 7 shows the different classifications of the membrane [10].

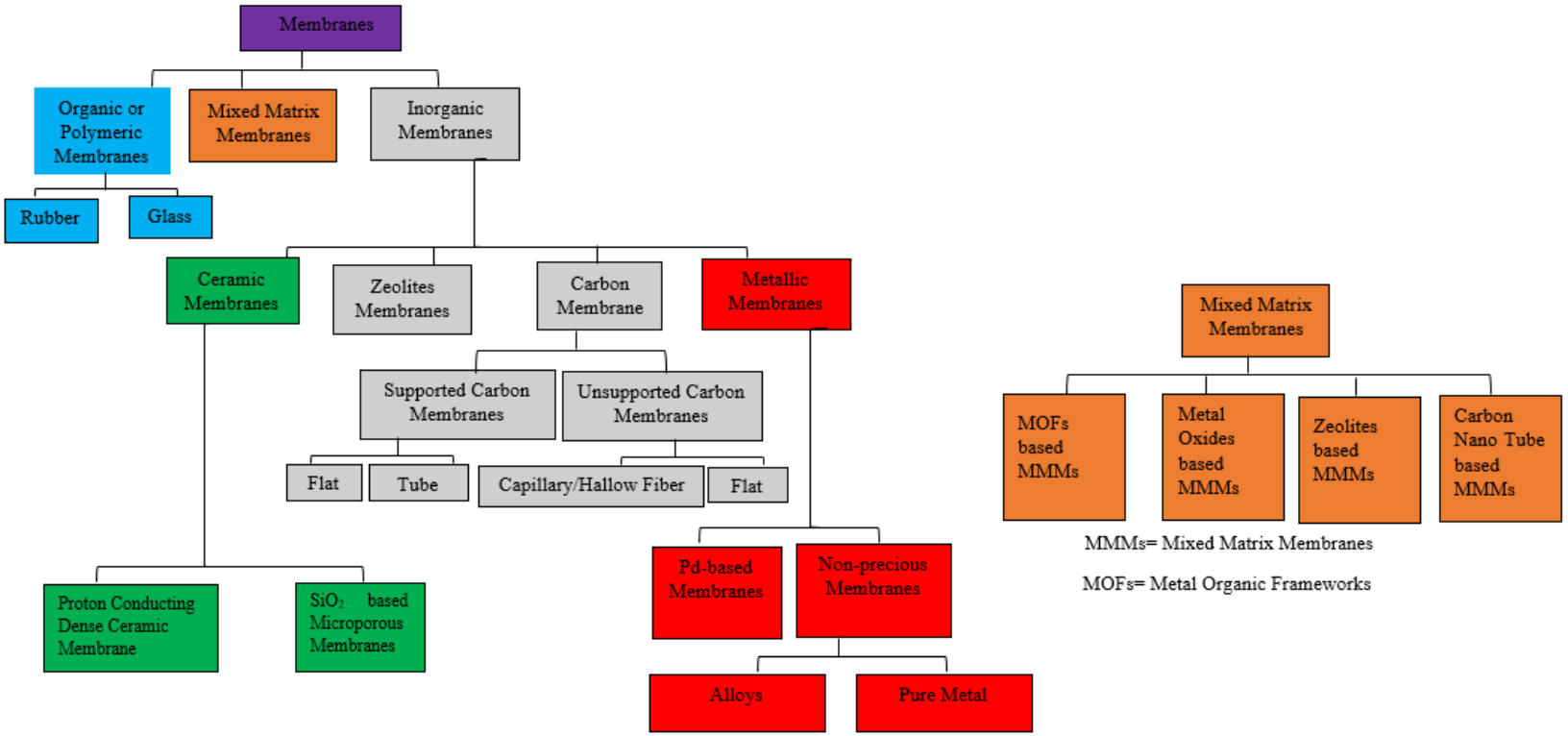

Figure 7. Membrane classifications

Among all the membranes, the zeolitic imidazolate framework (ZIF) exhibited an energetic gas separation performance. ZIF with a well-ordered porous structure, sub-nano size, and outstanding hydrothermal stability has been considered the most promising material for membrane applications. There are many types of ZIF membranes The most commonly used ZIF membranes for gas separation applications are ZIF-4, ZIF-7, ZIF-8, ZIF-62, ZIF-76, DD3R, FAU, and many others. Table 2 shows the advantages, disadvantages, and challenges of different types of ZIF membranes.

The zeolite membranes can be classified into two groups: in-situ growth and seeded growth membranes. Also, it can be classified based on synthetic processes such as aqueous synthesis at room temperature, vapor-assisted conversion, ultrasonic synthesis, the microemulsion method, electrochemical method, and microwave-assisted method [23]. The majority of zeolite membranes generate tetragonal plates that are not layer-by-layer grown, resulting in the substantial corrugation of the membrane layer. The presence of inter-crystalline pores which diminish the effectiveness of molecular separation is the primary challenge in the production of zeolite membranes. The followings are the steps for gas penetration and gas transfer through a zeolitic membrane: Firstly, adsorption from the bulk phase to the zeolite's exterior surface occurs. Secondly, diffusion from the surface to the inside of the zeolite channel happens. Then, diffusion inside the zeolite channel happens. Finally, diffusion from the zeolite channel to the external surface and desorption from the external surface into the gas phase would occur [24].

Among all of these ZIF membranes, recently ZIF-8 membranes have become attractive because it provides more efficient separation results as compared to other ZIF membranes [25]. Microwave-assisted solvo-thermal and secondary growth were used to produce ZIF-8 membranes in a variety of ways. To build a polycrystalline structure, a secondary growth mechanism is used to create nucleation sites on the support [26].

In most cases, ZIF membranes are supported by porous ceramic support. The ceramic frameworks exhibit high convective heat transfer and high chemical and structural stability. They have a low pressure drop, high turbulence, and high external mass transfer rate. The high cost of ceramic support, as well as the presence of impurities, has posed a significant impediment to industrialization. The effects of the porous support, sweep gas, and concentration polarization can also have a substantial impact on the membrane's separation performance [27].

Table 2.Different types of ZIF membranes

Zeolite Membranes Type	Advantage	Disadvantages	Challenges
ZIFs	Zeolite membranes have no cracks or pinholes. They are extremely thin and showing a good high hydrogen permeability [28]. At temperatures ranging from 25 to 700 degrees Celsius, hydrogen gas can be separated by zeolite membranes. [29].	Zeolite membranes have a pore size considerably big compared to the kinetic diameter of hydrogen gas. So the employment of them for separating hydrogen gas from other light gas molecules is challenging [38].	The zeolite membranes have layered structure that are fragile and difficult to manufacture [38]. One of the most important challenges is to maintain their structural integrity at temperatures of up to 150 degrees Celsius [40].
ZIF-8	The defect-free ZIF-8 membranes have been developed successfully by incorporating polydopamine in aqueous solutions [26]	In ZIF-8 membranes, thick layer of membrane improves the mass transfer resistance for the gases but it usually showed low permeance for hydrogen gas [39]. The low selectivity of ZIF-8 membranes for hydrogen separation makes them limited to be utilized [40].	As the feed pressure increased in ZIF-8 membranes, the amount of gas molecules that are adsorbed and diffused also increased [45] .
DD3R	Due to the structural property, DD3R membranes are not affected by changes in temperature or chemical condition [30]. DD3R was not degraded by H_2S gas for longer than 1000 hours. [31].	In DD3R membranes, the selectivity of mixtures of weakly adsorbing components was independent of pressure [30].	In DD3R membranes, as the temperature and pressure increased, the selectivity of mixtures of strongly and weakly adsorbing components decreased [30].
NaA	NaA zeolite membranes are thermally and chemically resistant in severe conditions due to their well-organized structure [32].	The production of NaA zeolite membranes typically took place via a process known as a secondary growth which requires the use of support surfaces [41]. Some of the support materials have a negative zeta potential that causes an electrostatic interactions, especially repulsion [38].	The main obstacle to the use of NaA zeolite membranes for large-scale applications is high fabrication costs [41].
SAPO-34	Silicoaluminophosphate (SAPO-34) has been employed in membrane reactors at high temperature (200–600 °C) [33].	In the presence of water, SAPO-34 membranes were less effective at room temperature [33].	After being exposed to a hydrothermal environment, the commonly used ceramic substrate as a support layer experienced decomposition [46].

FAU	Faujasite (FAU) zeolite membranes exhibit excellent catalytic and ion-exchange capabilities [34].	In the preparation of FAU membranes, direct crystallization via single stage in-situ synthesis usually resulted in non-homogenous zeolite layer [42].	At 373 K, FAU membranes showed negative expansion coefficients which causes thermal stress and the formation of cracks inside the membrane layer [42].
MFI	At high temperature (300-600 °C), MFI membranes exhibit steam or water to sieve from gas molecules [35].	The presence of such gases as C_2H_4, C_2H_6 in the industrial stream affects the hydrogen permeability [31].	At high temperatures, there was only minor dependency of the membrane properties on the feed pressure or the water vapor pressure [47]. Also, MFI membranes exhibit a sintering effect at high temperature [35].
UIO-66	For the UiO-66 membrane, a benzene dicarboxylic acid series that includes amino, nitro, and carboxyl groups is a good candidate for use as a ligand [36].	UIP-66 (Universitet I Oslo) has a relatively large pore size of 6 Å that reduces the molecular sieving properties of the membrane [43].	During the manufacturing process for membranes, the complex formation of zinc ions with the linker creates the reverse hydrolysis effect [48].
Zeolite-MOFs Membrane	The gas permeation flux is approximately proportional to the transmembrane pressure drop [37]. Hydrogen gas flux can easily be improved by increasing the feed pressure.	Gases should encounter a net attraction force when their molecular size is smaller than the MOF channel diameter [44].	When hydrogen gas is mixed with gases that have a greater kinetic diameter, the permeability of the hydrogen gas is decreased because of the repulsive force that exists between the two types of gases [44].

Recently attempts have been made to develop metal organic framework based ZIF (MOF-ZIF) membranes. Due to their molecular sieving capabilities, metal organic frameworks (MOFs) are regarded as an appropriate filler for producing mixed matrix membranes (MMMs). MMMs have been successfully commercialized due to their strong hydrothermal stability and acid or alkali resistance. MOFs belong to the 2nm micro regime, which denotes the extremely small nanometer-scale pores required for molecular sieving of smaller gas molecules from bigger gas molecules. These membranes are attractive because they are inexpensive, mechanically stable, and resistant to high temperatures and high pressure. When there was a big difference in pressure between the feed and the permeate sides, MMMs showed enhanced gas permeability [49]. A defect-free interface can be generated in MMMs by optimizing the interfacial architecture. When the loading of MOF nanoparticles is increased in the MMMs, the application of MMMs is limited because the dispersion of MOF particles is not easy in MMMs. Increased filler loading improves penetrant-filler interaction and increases separation from the membrane, which is also responsible for particle agglomeration [50]. Table 3 shows the permeability and selectivity of zeolites mixed matrix membranes and MOF based ZIF membranes.

When the gas stream contains water vapor, the hydrothermal stability of the membranes is compromised. For this purpose, silica is added to the membrane composition. Silica has a hydrophilic site that allows water to easily react with it and form thin films, causing chemical and microstructural instability [51]. AS has a surface area of 510–970 m^2g^{-1} and a pore diameter range of 15–20, which makes it useful for separation processes [52]. Because AS are microporous crystalline materials with homogeneous pores and channel diameters, incorporating them has generated a lot of interest in membrane technology. The incorporation of AS improves interfacial void formation, gas transport phenomena, and pore blockage. Filler precipitation may happen during the preparation process because of the differences in the physical and chemical properties of fillers. The membrane's extra porosity provides an additional transport mechanism that improves the membrane's non-ideal performance [53].

Table 3. Permeability and selectivities of Zeolites and MOF based mixed matrix membranes

	Polymers	Additive	Loading (wt.%)	Temp (ºC, K)	Pressure	Permeability (Barrers)	Selectivity	Ref
Zeolites based mixed-matrix membranes	PDMS	Silicate-1	50	15ºC	1.013 bar	CO_2 = 2760 CH_4 =501	CO_2/CH_4 = 5.50	[54]
	6FDA-6FpDA-DABA polyimide	L	20	35ºC	8 atm	CO_2 = 19.60 CH_4 =0.50	CO_2/CH_4 = 39.20	[55]
	Udel®	Nu-6 (2)	14.7	25ºC	538 kPa	H_2 = 35.8 CH_4 = <0.09	H_2/CH_4 = >398	[56]
	PES	NaA	50	35ºC	10 atm	CO_2 = 1.1 CH_4 = 0.0185	CO_2/CH_4 = 59.60	[57]
	PDMC	SSZ-13	15	35ºC	65 Psia	CO_2 = 88.6 ± 4.4	CO_2/CH_4 = 41.90 ± 0.7	[58]
	PDMS	Zeolite 4A	40	35ºC	-	H_2 = 9516 CO_2 = 2945	H_2/CO_2 = 3.23	[59]
	PI	Zeolite 4A	30	25ºC	10 bar	CO_2 = 13.28 N_2 = 0.4608	CO_2/N_2 = 28.82	[60]
	PI	ZSM-5	20	25ºC	10 bar	CO_2 = 19.194 N_2 = 0.5376	CO_2/N_2 = 35.70	
	PDMS	ZSM-5	38	-	-	CO_2 = 5464 ± 270 N_2 = 442 ± 22	CO_2/N_2 = 12.40 ± 0.6	[61]
MOF based mixed-matrix membranes	CA	ZIF-8	5	25ºC	4 bar	O_2=3.36±0.124 N_2=0.35±0.125	O_2/N_2=9.58±0.18	[62]
	6FDA-DAM Polyimide	ZIF-90	15	25ºC	2atm	CO_2=720	CO_2/CH_4=37	[63]
	PBI	ZIF-7	50	35ºC	3.5 atm	H_2=26.2 CO_2=1.8	H_2/CO_2=14.90	[64]
	Pebax	ZIF-7	34	20ºC	3.75 bar	CO_2=39 GPU	CO_2/CH_4=44	[65]
	Pebax 2533	ZIF-11	10	20ºC	2 bar	CO_2=230	CO_2/N_2=53	[66]

1.2 Research objective

To overcome the trade-off between permeability and selectivity, an approach to incorporating inorganic fillers such as zeolites, MOFs, and carbon molecular sieves into a membrane matrix has been tested. In this study, alumino-silicate (AS) and activated carbon (AC) were prepared and incorporated into the ZIF. AS is generally crystalline microporous material with unusual pore and channel diameters. The prepared membrane (ZIF-AC-AS) was tested for various gases such as H_2, CO_2, and CH_4.

In this study, the effect of the vertical or horizontal position of the disc in the autoclave was investigated. The results showed that it had a great impact on the depth of the layer. The precipitation of fillers was also studied. Filler precipitation may occur during the preparation process due to differences in physiochemical characteristics and density of fillers. That can cause the formation of a separate inhomogeneous layer between the filler and polymer phase. The selectivity of a material is a function of its qualities under certain operating conditions and in the absence of cracks. When the cracks are present in the membrane, gases pass through the membrane without separation due to the viscous flow. The prepared membranes were tested at room temperature and 100 ºC to investigate the effect of the temperature on permeability. As the temperature rises, it would affect the permeability of H_2, CH_4, and CO_2 gases.

Chapter 2. Materials and Methods

The chemicals such as zinc nitrate hexahydrate (Zn $(NO_3)_2.6H_2O$)), methanol (CH_3OH), 2 methylimidazole (Hmim), zinc chloride ($ZnCl_2$), sodium formate ($NaHCO_2$), phosphoric acid (H_3PO_4) and zinc chloride solution were purchased from the manufacturer.

2.1 Synthesis of Alumino-Silicate (AS) and Activated Carbon (AC) from algae

In Figure 8, Brown algae, green algae, and Quercus alba were collected from the Busan River and Arisu water filtering plants, respectively, and excess water was removed using filter paper. To evaporate the moisture, the algae were placed in direct sunlight for 3–4 days. Then, it was dried in an oven for 5 hours at 105 °C to remove any remaining moisture. The dried algae were crushed and sieved through a sieve with a mesh size of 150. A very fine powder was obtained. The H_3PO_4 was utilized as an active agent for brown algae, which modified the raw material's thermal properties. At room temperature, the absorption period of H_3PO_4 (wt 50%) into the powder obtained from the dried sample was 16 hours. Fine biomass powder of green algae was added to the $ZnCl_2$ activation agent for 24 hours to achieve absorption. The biomass powder and activation agent had the same weight ratio (1:1) in both samples. The absorption material was then calcined for 2-3 hours in a box resistance furnace at 500–600 °C. The excess H_3PO_4 was rinsed out of the brown algae-based char with distilled water until a neutral pH level was achieved [67]. The green algae-based char product was rinsed with a 3 M HCL solution to remove the zinc and free chlorine ions and then washed with distilled water until the neutral pH was achieved. The AC and AS materials were dried in an oven at 105 °C for 1 hour. Figure 9 shows the steps involved in the preparation of AC and AS.

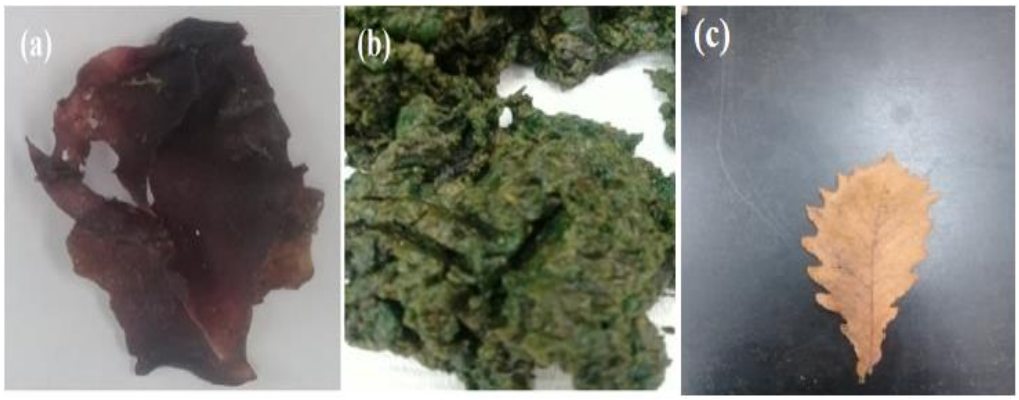

Figure 8. Source of AC and AS

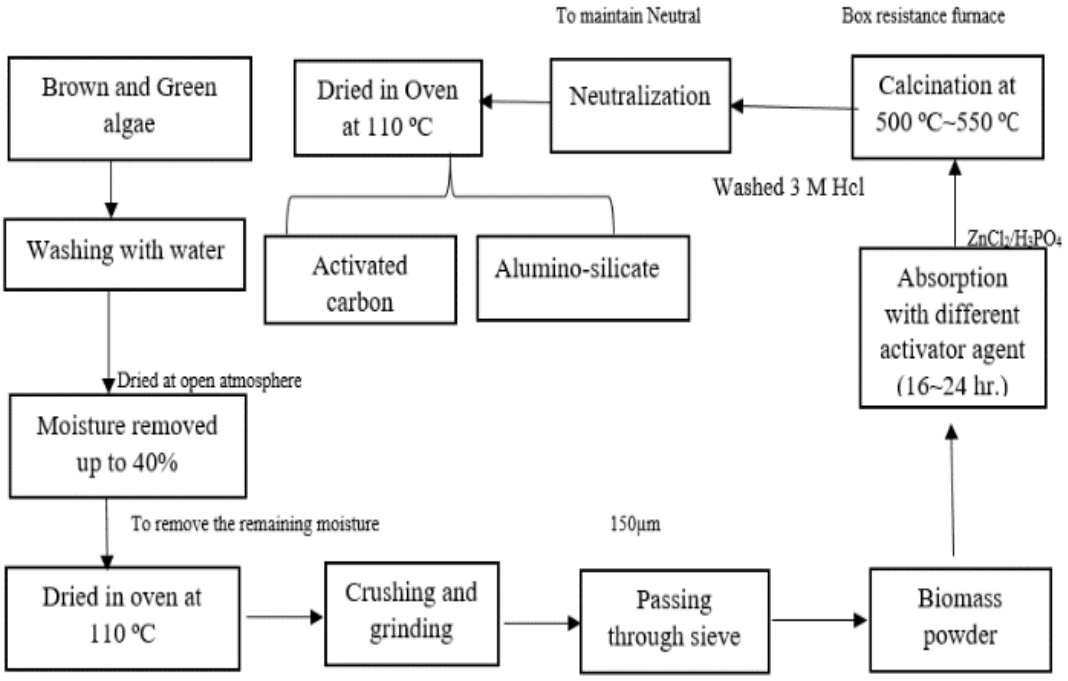

Figure 9. Preparation procedure of AC and AS [67]

2.2 Membrane fabrication

2.2.1 Seed synthesis

The ZIF-8 crystals were made using the Cravillon *et al*. method. In brief, 0.4175 g of Hmim and 0.3686 g of $Zn(NO_3)\cdot 6H_2O$ was dissolved in 25ml of methanol. After that, the Hmim solution was stirred into the Zn solution for 30 minutes at ambient temperature. The solution was then aged for 24 hours in a static environment to create colloidal ZIF-8 seeds. The solid crystals generated via solid crystal formation were collected by centrifugation at RPM 5000 for 20 minutes and cleaned three times with methanol. The collected particles were then dried overnight in a vacuum oven at 50 degrees Celsius. Finally, the ZIF-8 powder was dispersed in methanol under ultrasonication to yield a 0.1 wt percent seeding solution [51].

2.2.2 ZIF-8 membrane fabrication and post-treatment

A porous @-alumina disc support of 2 mm thickness, 1.4 µm pore size, 55.0 porosity percentage, and 25 mm diameter was purchased from Nishimura Advanced Ceramics Co., Ltd. (Japan). The Al_2O_3 was utilized as a thermally stable (maximum 1100 ºC) support and as a precursor in the formation of a composite with the ZIF particle [48]. The support was polished using sandpaper (mesh size 1600) and then washed in an ultrasonic water bath before seeding to achieve a smooth seeding surface. The support was then dried for 24 hours at 120°C in the oven. The disc was then dip-coated in the prepared seed solution for 10 seconds twice and dried overnight in an oven at 80 ºC. The thickness and structure of the membrane have a significant impact on species diffusion. With the addition of AC and AS particles, the secondary growth solution was created. Under ultrasonication, 0.0372 AC, 0.1286 g AS, 0.5460 g $ZnCl_2$, 0.2781 g $NaHCO_2$, and 0.4698 g Hmim were dissolved in 40 ml methanol and agitated for 30 minutes [51].

The samples were then aged for 24 hours before being placed into a Teflon-lined autoclave with the seed support loaded vertically. The autoclave is placed in a 120 °C oven for 6 hours. The autoclave was then allowed to cool to ambient temperature. Finally, the membrane was removed, washed with methanol, and dried for 24 hours at room temperature [51]. Figure 10 shows the experimental steps involved in the preparation of the membrane and Figure 11 shows the prepared membranes.

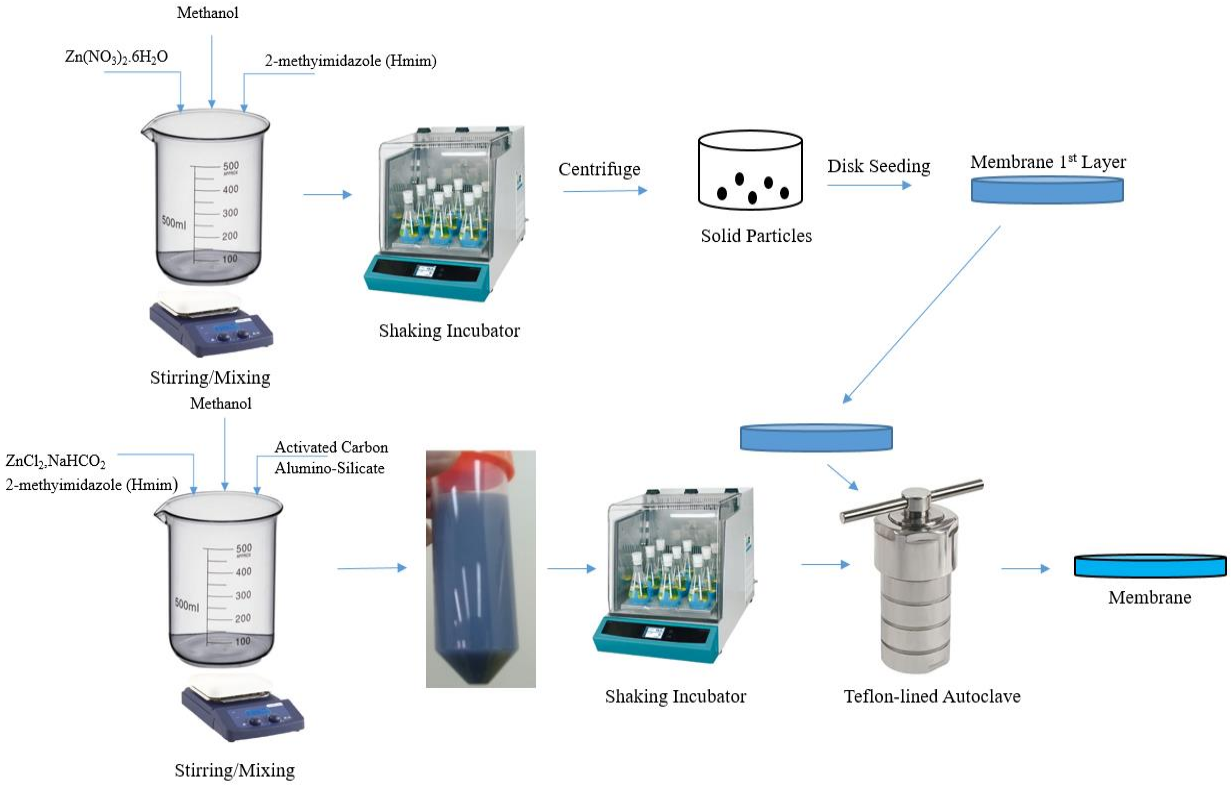

Figure 10. Experimental procedure for preparing the membrane[51]

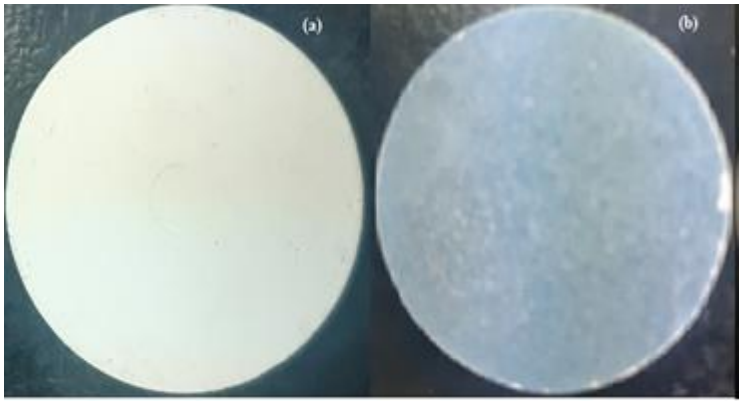

Figure 11. Prepared membrane ZIF (a) and ZIF-AC-AS (b)

2.2.3 Gas permeation test and characterization

The schematic diagram of the gas permeation test is shown in Figures 12 and 13. The gas permeation test was carried out at room and 100 ºC temperatures. The membrane was loaded into the permeation cell with the Teflon O-ring on the outside and on the top side. Before testing, the membrane was activated with argon gas. The feed flow rate was set at 65 sccm, and the total pressure was kept at around 3 bars, with the help of a ball valve (controlling the feed and the retentate side). The permeation test was carried out for 50 minutes. On the permeate side, argon gas (sweep gas) was utilized to dilute the gas concentration while maintaining a pressure of 1 bar. By assuming zero partial pressure of the species on the permeate side, sweep gas was utilized to boost the driving power for permeation and carry away the species on the permeate side. The sweep gas flow rate has a considerable impact on separation success. The pressure shift causes ZIF's structure flexibility to be disrupted, which affects the adsorption isotherm process in the membrane. A gas chromatograph machine was used to examine the gas composition of the permeate and retentate [51]. Figure 14 shows the schematic permeation experimental setup for the membrane [68].

Unfortunately, the syngas composition, the same as in the industrial coal gasification products, was not technically available in the lab due to safety issue. Therefore, for the lab-scale experiment, the mixture of gas composition for CO_2/CH_4 and H_2/CH_4 to be 50% each was tested. If industrial syngas composition is tested, then a cyclic membrane testing set-up would be required. Figure 15 explains how the cyclic membrane testing system works for gas purification.

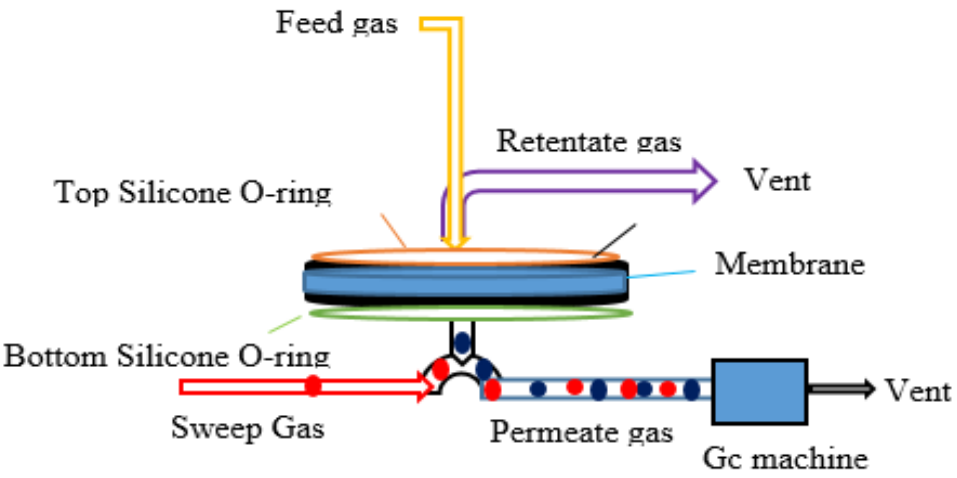

Figure 12. Schematic diagram of membrane O-ring layout

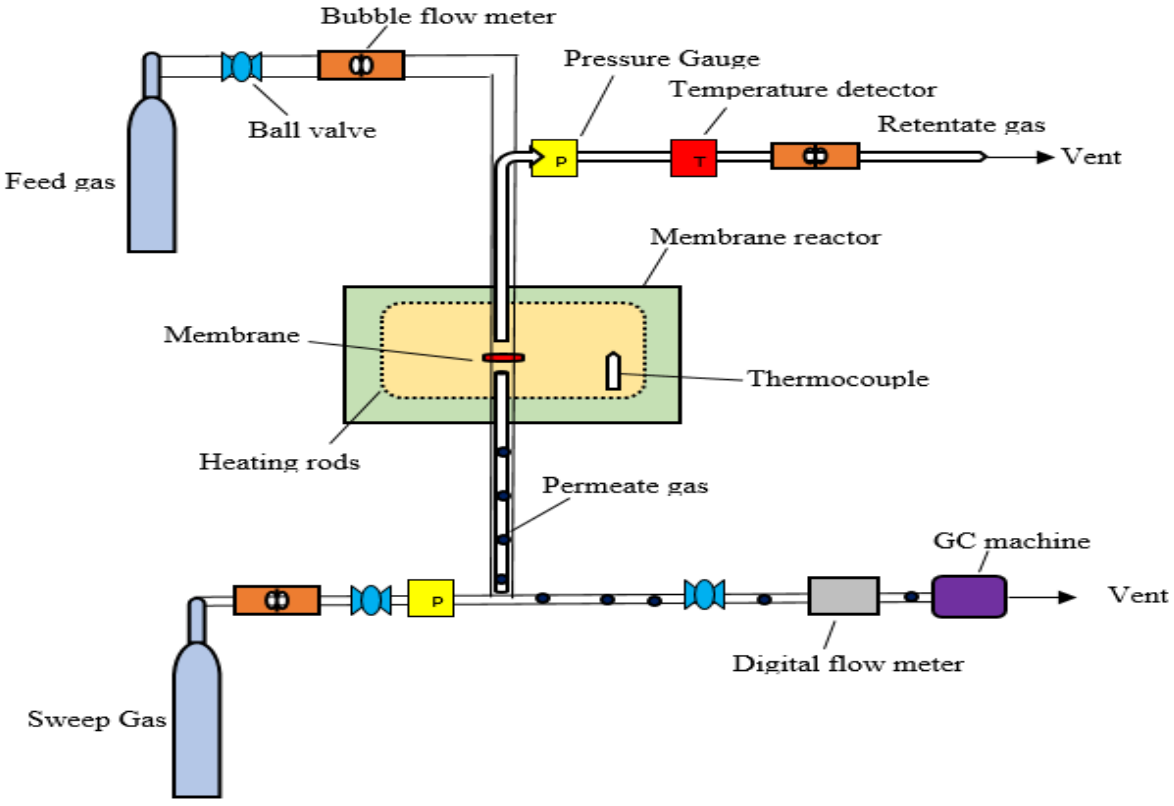

Figure 13. Schematic diagram of membrane testing unit in lab scale

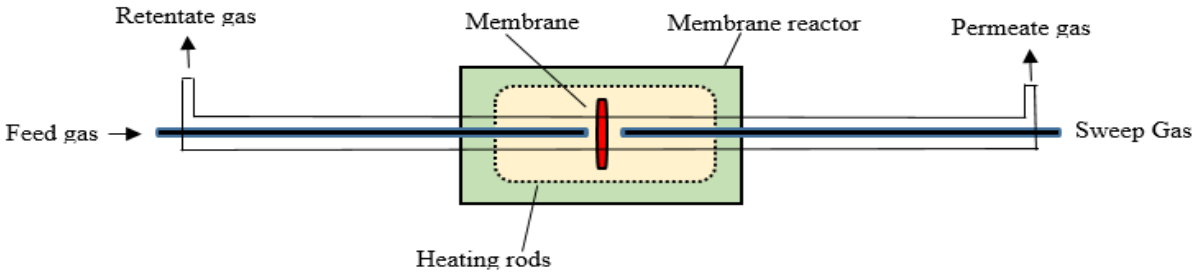

Figure 14. Gases flow pattern through membrane lab scale [68].

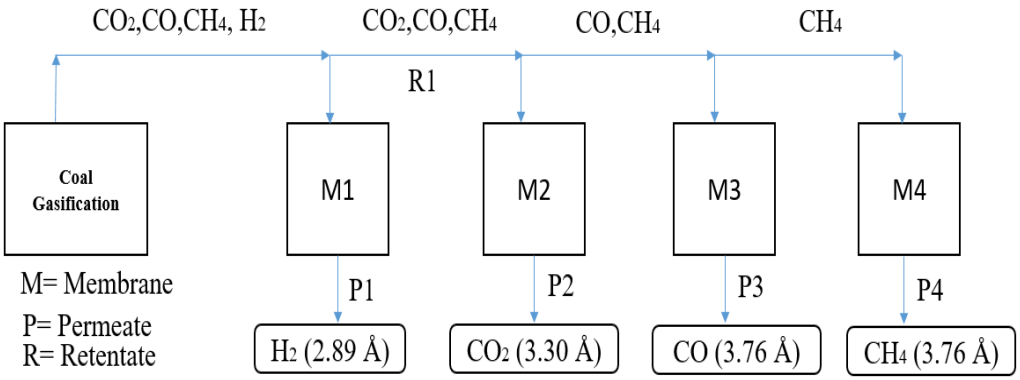

Figure 15. Cyclic layout of membrane requirement for gases separation

The incorporation of AC and AS was adjusted according to the volume basis. The AC was prepared by using H_3PO_4, KOH, $ZnCl_2$, and $FeCl_3$, but an equal amount of prepared carbon exhibits different volumes. If the incorporation is carried out on the basis of weight, then the mixing is not homogeneous and it makes the same particles agglomerate. Therefore, to maintain a well homogeneously mixed solution and avoid particle agglomeration, a 1:1 ratio (ZIF: AC and AS) was prepared. Figure 16 shows the samples bottles with 1 mL volume. The weight of the AC made with KOH was 0.0398 grams, but the weight of the same AC made with $ZnCl_2$ was 0.7856 grams.

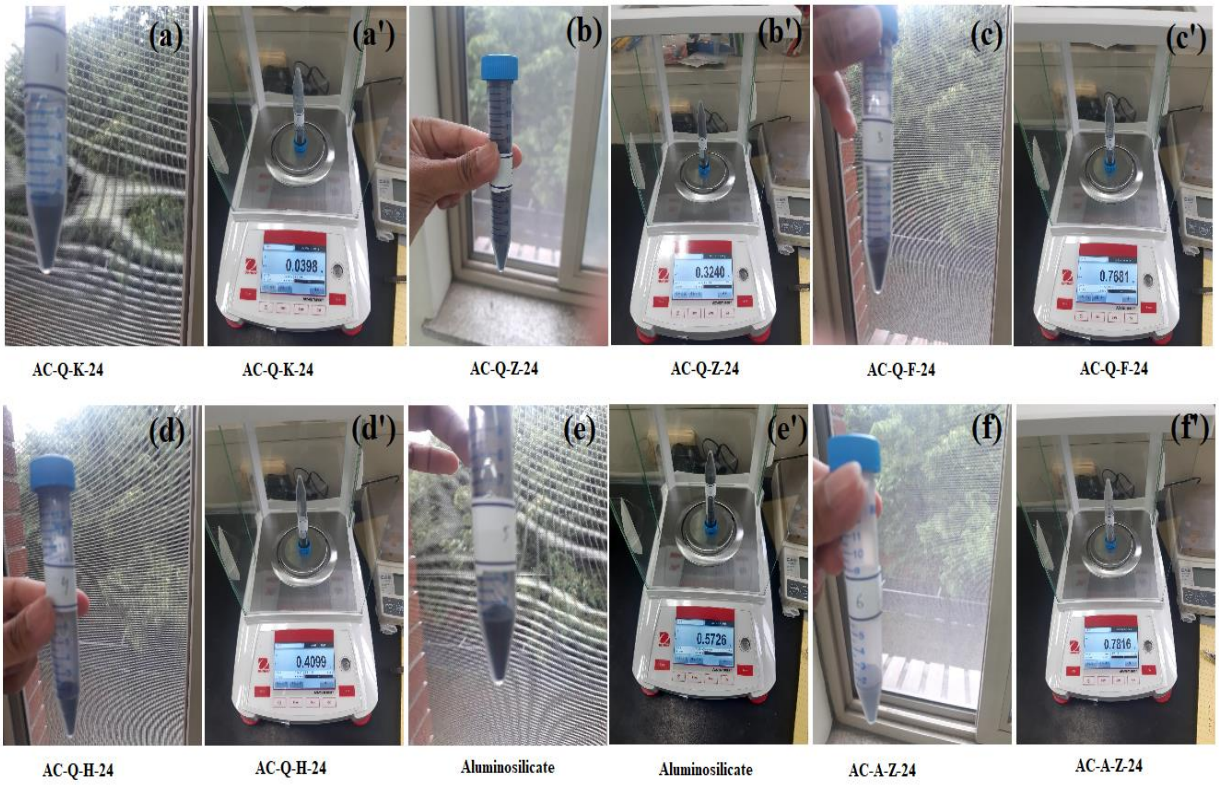

Figure 16. Volume and weight ratio of AC and AS

The homogenous mixing of AC and AS in the solution of ZIF is to be considered very important for the uniform growth of the layer on the top of the support disc. In this study, the prepared AC occupied more volume space as compared to ZIF particles. Figure 17 (a) shows that when the same volume of AC and AS was mixed with ZIF particles, a homogenous mixture was formed. As shown in Figure 17 (b), when the volume of AC and AS increased and was greater than the ZIF particles, precipitates were formed.

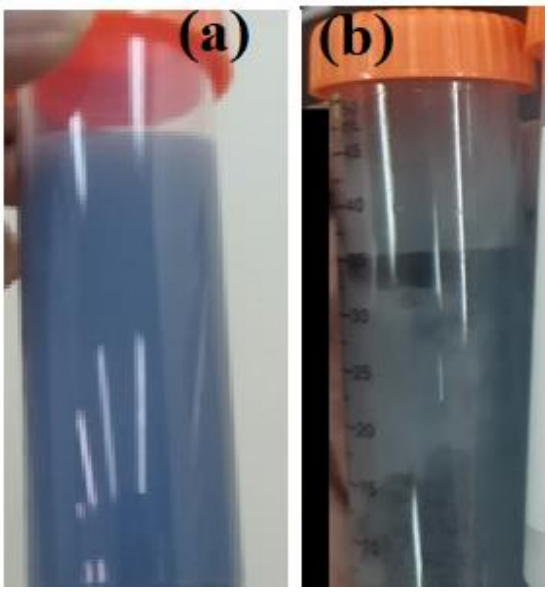

Figure 17. Uniform mixing (a) and precipitation of filler (b)

Chapter 3. Results and Discussion

3.1 AC characterization

To determine the properties of the prepared AC, several characterization approaches were applied. The Brunauer–Emmett–Teller (BET) technique was used to examine the surface area (SBET) of AC. The Micromeritics Flow Prep was used to examine the N_2 adsorption-desorption of produced ACs at -196 °C (Gemini V-060). Quercus Alba was tested for nitrogen adsorption at 77 °C. To clean all of the pores, all of the samples were evacuated under a vacuum at 150 °C for an overnight period. The samples were then degassed for 6 hours at 150 °C with a nitrogen flow. A scanning electron microscope (SEM) with energy dispersive x-ray (EDX) analysis was used to assess changes in surface morphological features (SEM-EDX, EM-30AX, COXEM Korea).

The x-ray diffraction (XRD) technique was used to determine the crystal structure (Smart Lab Rigaku, Japan). An organic element analyzer was used to determine the presence of elements (C, P, O, Fe, Cl, Na, and Ca) in prepared AC. Fourier transform infrared spectroscopy (FT-IR) (TENSOR27 Bruker Germany) spectrum approach was used to detect the functional group. Thermogravimetric analysis (TGA) was used to look at how the thermal degradation change (Model: 701 Leco).

3.1.1 Scanning electron microscopy (SEM) analysis of AC

The scanning electron micrographs shown in Figure 18 demonstrate that the raw "Quercus Alba" has a wide diversity in particle shapes and sizes. In the structure of the raw precursor shown in Figure 18(b), no pores was observed. The pores shown in Figure 19 would be formed as a result of the application of H_3PO_4 as an activator agent during the AC manufacturing procedure [69-70].

Figure 20 demonstrates that the formation of cylindrical holes occurred as a result of the use of $ZnCl_2$ as an activator agent. When KOH was used as an activator agent, an enormous number of macropores were produced in the AC as shown in Figure 21 [71]. External surface cracks were produced as shown in Figure 21, when $FeCl_3$ was applied as an activator agent to treat the material. It is possible that the volatile molecules will be released from the interior of the structure, which can cause the structural changes [72].

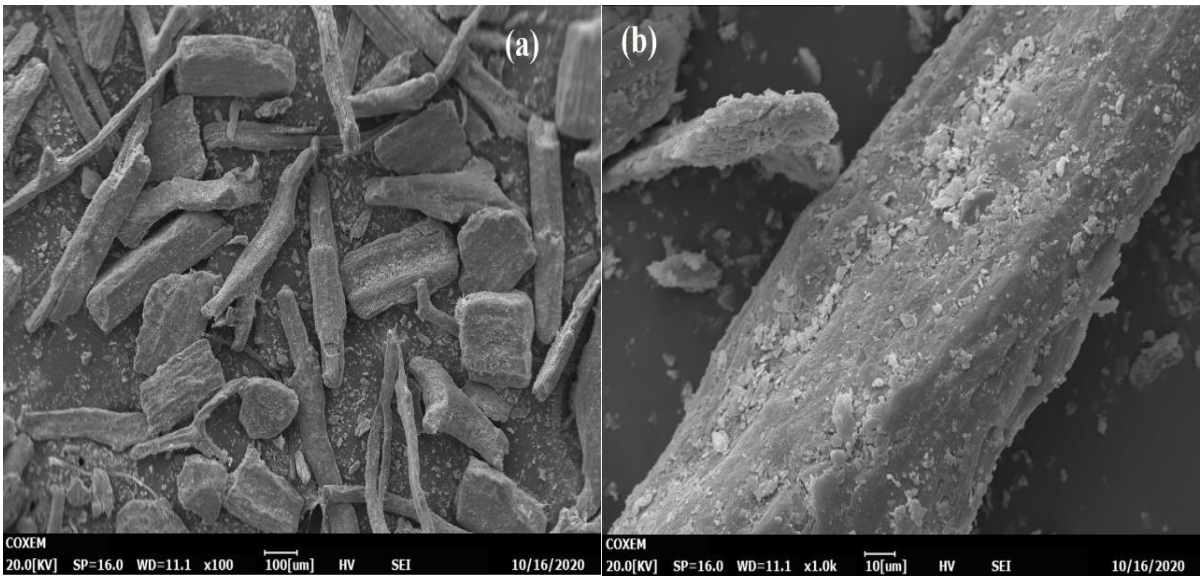

Figure 18. SEM image of raw Quercus Alba

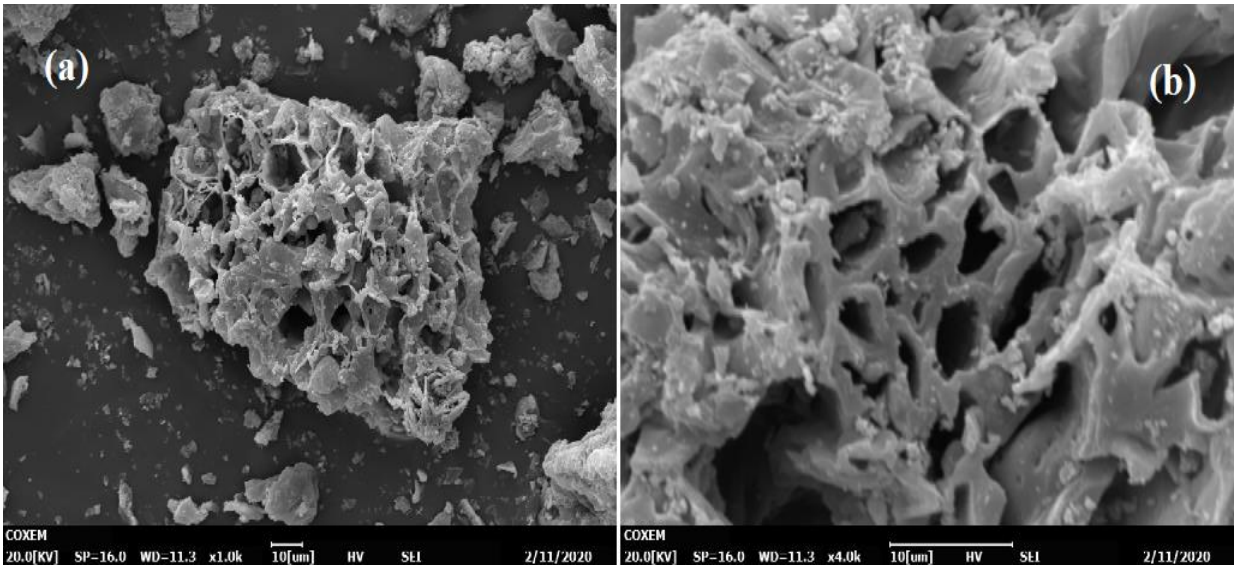

Figure 19. SEM image of AC by using H_3PO_4

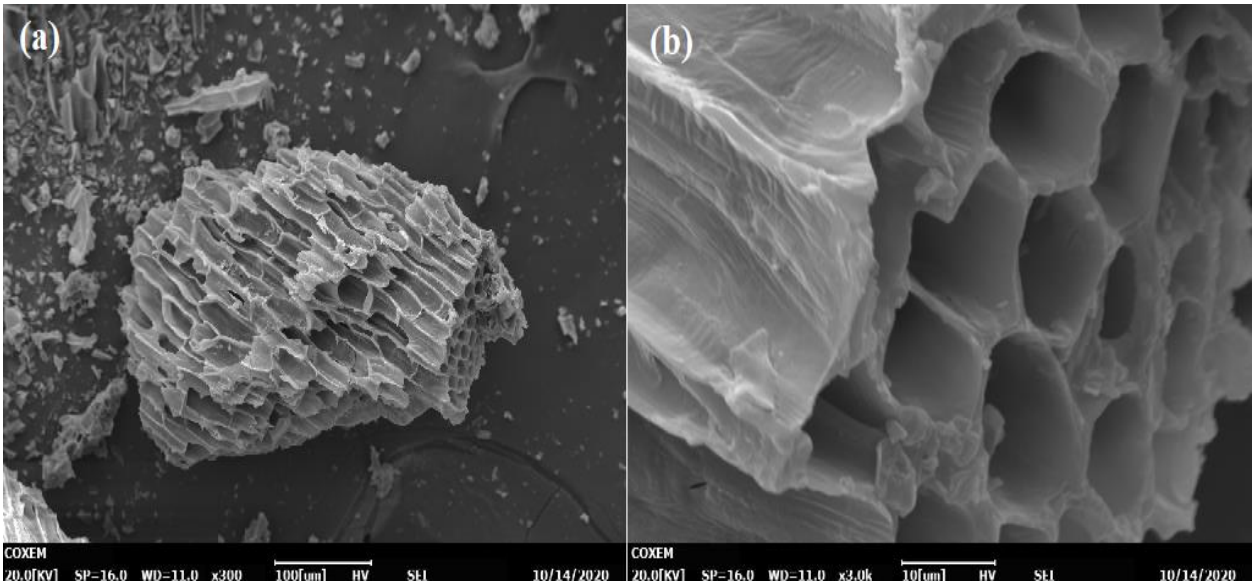

Figure 20. SEM image of AC by using $ZnCl_2$

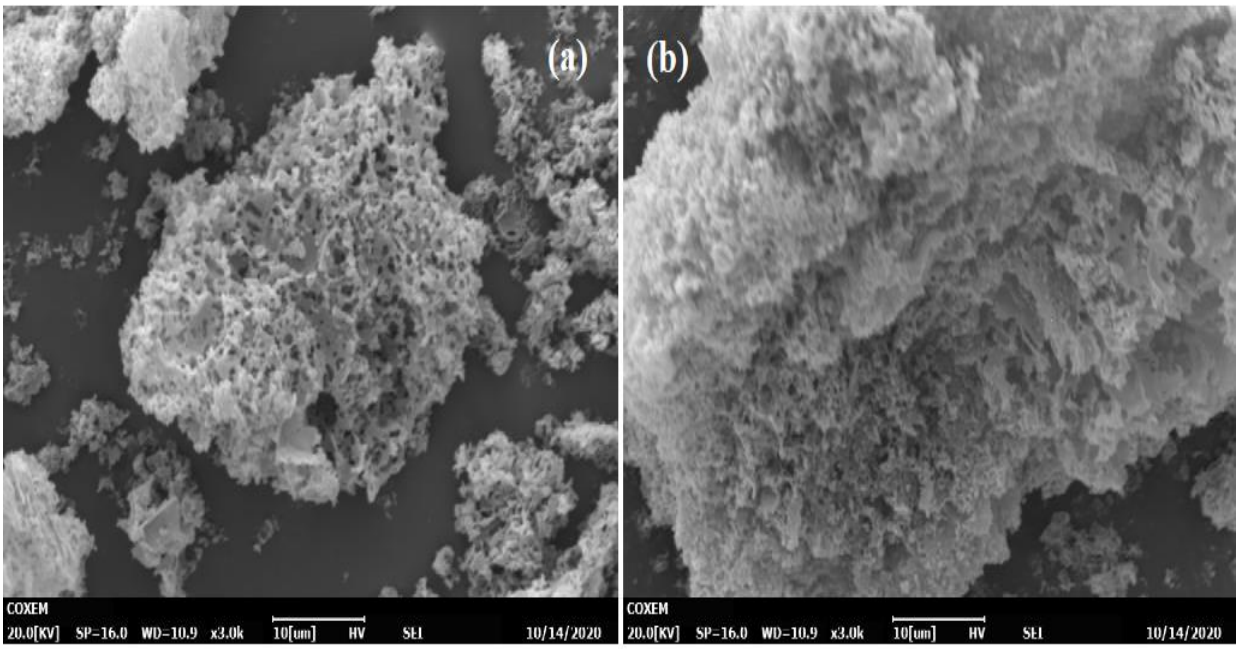

Figure 21.SEM image of AC by using KOH

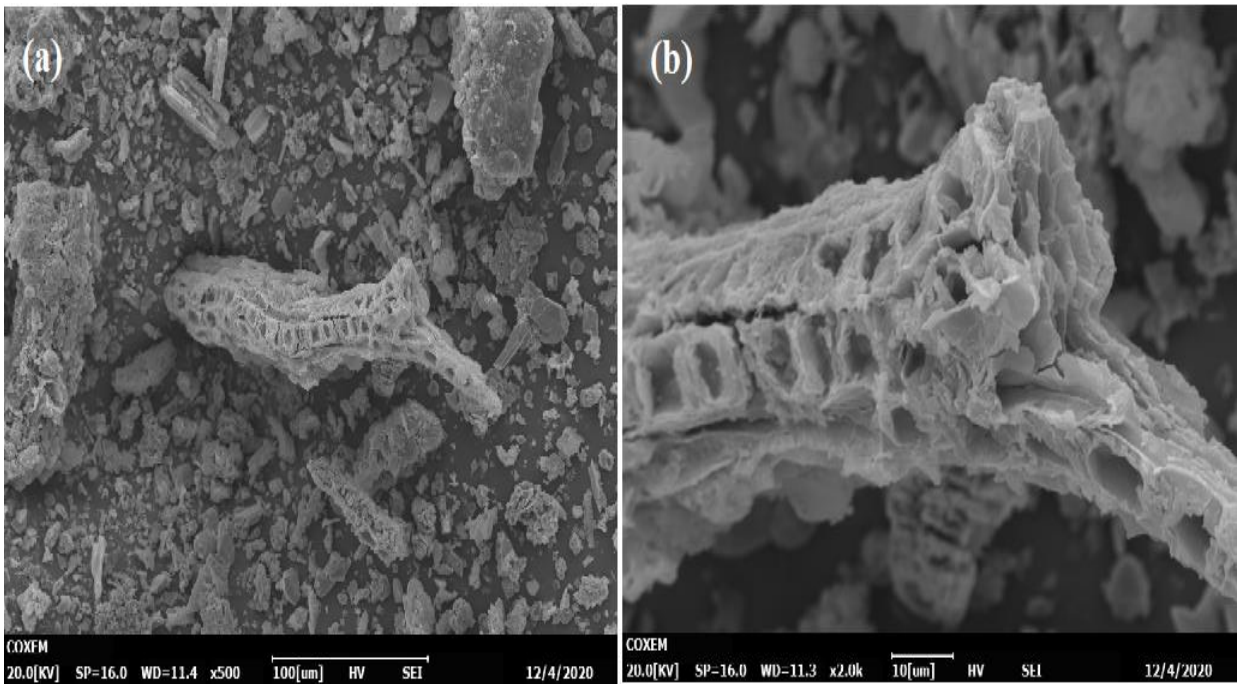

Figure 22. SEM image of AC by using $FeCl_3$

3.1.2 Energy Dispersive X-ray (EDX) analysis of AC

Table 4 shows the EDX elemental analysis result of the produced ACs. The carbon content rose from 40 percent to 53 percent when the H_3PO_4 chemical activation was utilized. A little quantity of phosphor was also present in the H_3PO_4-based AC since phosphoric acid was used as the active ingredient. When zinc chloride was used as an activator, the carbon content was 57 percent. Compared to ACs made by other chemical agents, the oxygen content was significantly high.

The carbon content of the raw precursor rose to 73 percent when KOH was used as an activator agent and it was significantly higher than the carbon content of the other ACs in this study. When $FeCl_3$ was utilized as an activator agent for the ACs preparation, the carbon concentration was the lowest compared to other activators. The sample of $FeCl_3$-based AC had trace amounts of chlorine and iron as a result of the usage of iron chloride as an activator agent. However, unfortunately, the EDX results were not based on the exact quantitative data.

Table 4. EDX analysis of prepared AC with different absorption time by chemical activation

Sample ID	At (Day)	CT (ºC)	Ct (hr)	Composition				
				C	O	P	Cl	Fe
Q				39	61	0	0	0
AC-Q-H-24	1	500-550	3	53	29	17	0	0
AC-Q-Z-24	1	500-550	3	56	44	0	0	0
AC-Q-K-24	1	500-550	3	74	26	0	0	0
AC-Q-F-24	1	500-550	3	50	38	0	4	8

At= Absorption Time , CT= Calcination Temperature, Ct= Calcination Time

3.1.3 X-ray diffraction (XRD) analysis of AC

The XRD spectra of ACs that were manufactured using H_3PO_4, $ZnCl_2$, KOH, and $FeCl_3$ are shown in Figure 23. The peaks with unique shapes in Figure 23 (for AC-Q-H-24, AC-Q-Z-24, and AC-Q-K-24) at $2\theta = 23°$ show the existence of the carbonaceous structure in the prepared ACs. Based on the previous study, it is believed that the carbonaceous structure was present in all three of the ACs [67]. The termination of double bonds with hydrogen atoms might be the reason for the formation of the amorphous carbon structure of ACs [73]. For the AC-Q-H-24 sample, a very inconspicuous peak was observed at an angle of 15°. The use of H_3PO_4 as an activator agent resulted in the formation of a small peak at $2\theta = 15°$. This peak shows the presence of the element phosphor "P."

The production of polycrystalline Fe_2O_3 and Fe_3O_4 is reflected by the presence of a polycrystalline phase in the XRD analysis of $FeCl_3$-based AC (AC-Q-F-24). Some of the steep peaks detected at $2\theta = 33°$, 49°, and 57° may be attributed to the creation of Fe_3O_4 according to previously reported study [74]. In addition, the existence of these peaks suggests that the Fe_3O_4 particles were successfully seeded into the carbon matrix during the pyrolysis process [75]. On the other hand, Fe_3O_4 could be made by carbo-thermal reduction of Fe_2O_3 on a carbon surface [74].

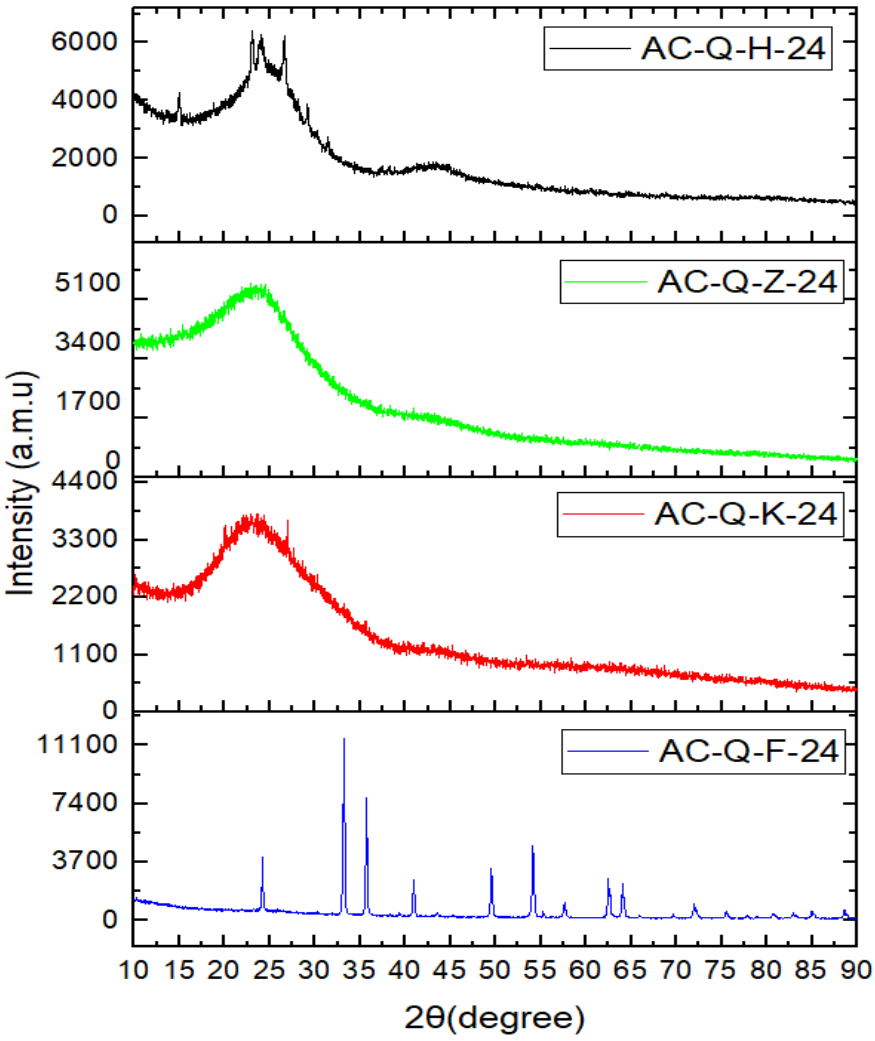

Figure 23. XRD analysis of AC by using different chemical activations

3.1.4 Brunauer-Emmett-Teller (BET) analysis of AC

Table 5 shows the BET surface area of ACs with various activation agents. The findings show that among the several activator agents used in this study, the surface area of AC activated by phosphoric acid was the largest (890 m^2/g). It is likely that a significant number of pores were formed as the reaction develops and P_2O_5 gases have been released [76]. The lignocellulose structure of Quercus Alba has a greater oxygen content. By interacting with oxygen, zinc chloride, an acidic reagent, catalyzes the dehydration process [77].

The AC-Q-Z-24 sample showed the lowest surface area of 5 m^2/g (at 550 °C) among all the investigated ACs. For AC-Q-K-24, the potassium and carbon dioxide did not entirely evaporate since the temperature was set at 550 °C, leaving an average surface area of 240 m^2/g. The surface area of the AC-Q-F-24 sample was also relatively small (35 m^2/g). When AC is produced via the ferric chloride activation method, it is typical for magnetic iron oxides such as magnetite (Fe_3O_4), hematite (Fe_2O_3), or other kinds of ferrite to precipitate together. It is well known that these magnetite and hematite particles clog the pores in ACs and reduce their pore volume and surface area [74].

Table 5. Represent the BET surface area derived from different activation agents

Sample ID	BET surface area (m^2/g)
AC-Q-H-24	890
AC-Q-Z-24	5
AC-Q-K-24	240
AC-Q-F-24	35

3.1.5 Thermogravimetric (TGA) analysis of AC

After undergoing thermal carbonization, the entire TGA analysis of the AC generated by Quercus Alba is shown in Figure 24. According to the results, the H_3PO_4-based AC began to degrade at a temperature of 300 degrees Celsius and continued to a temperature of 875 degrees Celsius. The $ZnCl_2$-based AC began to disintegrate at temperatures of 120 degrees Celsius and was fully destroyed at temperatures exceeding 780 degrees Celsius. According to the findings, the KOH-based AC began to degrade at the temperature of about 150 degrees Celsius and entirely disintegrated at the temperature of higher than 975 degrees Celsius. Around 280 degrees Celsius is when the $FeCl_3$-based AC starts to degrade, and 550 degrees Celsius is when it declines completely.

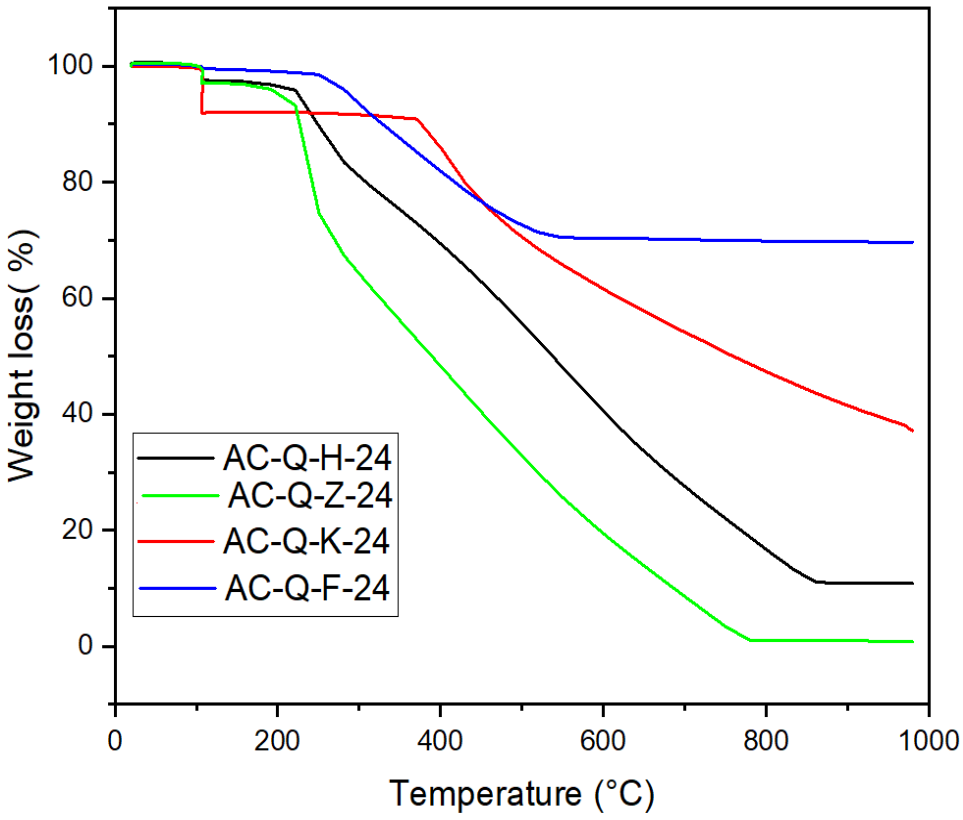

Figure 24. TGA analysis of AC by using different chemical activations

3.1.6 Fourier transform infrared (FT-IR) spectroscopy of AC

According to the results of the FT-IR analysis, the surface functional groups of the created AC are shown in Figure 25. The FT-IR research not only found evidence of oxidation but also provided insight into the nature of chemical bonds and their dissolution. The findings of the FT-IR analysis of the H_3PO_4-based AC suggested that C-O vibrations were responsible for the bonds measured at wavenumbers of 1078 cm^{-1} to 1141 cm^{-1}. The oxygen and phosphorus functionalities were responsible for the bonds that existed at a wavenumber in the range of 1000–1200 cm^{-1} (P-O-C). In addition, the C=C vibration was connected to the bond at above 1565 cm^{-1} [78], [79]. In Figure 25, the C-O stretching vibration was seen in ester and alcohol groups in the $ZnCl_2$-based AC sample. This vibration was observed in the bonds at 1095 and 1184 cm^{-1}. According to the findings of the EDX (Table 4), this stretched oxygen compound has the greatest presence of all the ACs that were synthesized. The bond that has a wavenumber of 1585cm^{-1} provides evidence that aromatic ring stretching is present. The bond that occurs at a frequency of 2350 cm^{-1} is due to the vibration stretching that occurs in alkyne groups. The bonds that are located at 2893 and 3080 cm^{-1} [80] provide evidence that an aliphatic–CH stretch is present. In the FT-IR results for the KOH-based AC sample, a strong bond close to 1584 cm^{-1} might be due the C=C aromatic ring stretching vibration [81]. There is a connection between the C-H stretching that occurs as a result of vibration in the alkynes group and a week-bond that has a wavenumber of 2348 cm^{-1} [82]. The bond at a wavenumber of 3363 cm^{-1} is connected to the OH stretching, which signals the vibration of the hydroxyl group [82]. In $FeCl_3$-based AC, the bonds at wavenumbers of 442 and 523 cm^{-1} were connected to the Fe-O vibration bonds. This was because the surface oxygen group was converted into iron oxides (Fe_3O_4) [74]. These Fe-O stretching vibrations might be caused by the octahedral and tetrahedral sites of magnetite [83]. The C=C bond in aromatic rings is established at a frequency of 1579 cm^{-1} and is caused by a stretching vibration. Also, the C-H stretching can be explained by the bond at 2986 cm^{-1} [74].

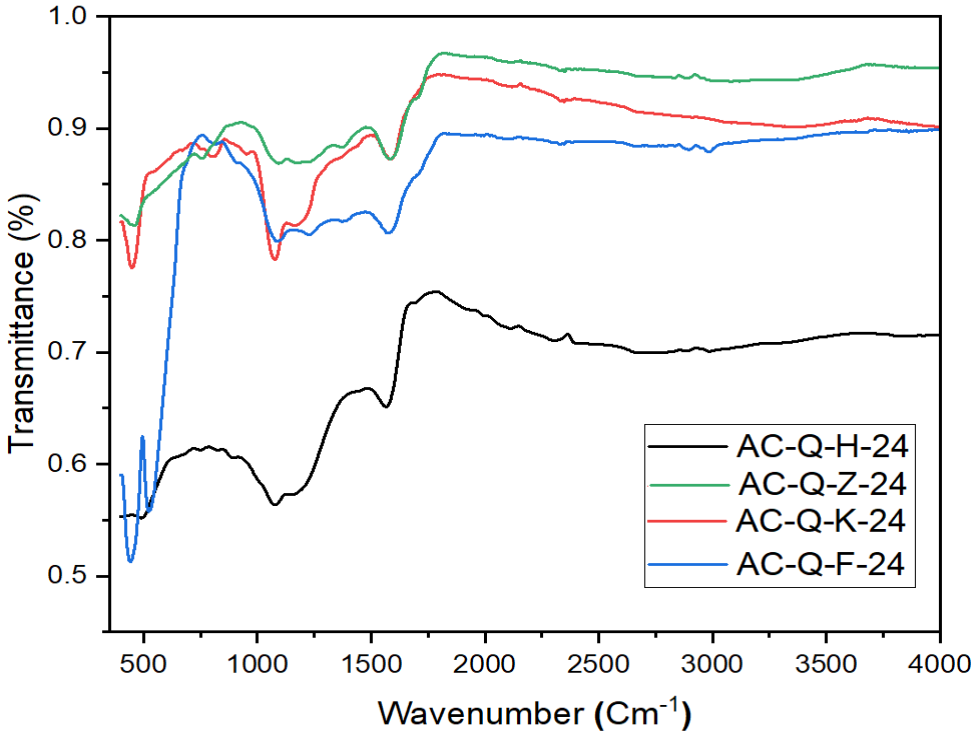

Figure 25. FT-IR analysis of AC by using different chemical activations

3.2 AS characterization

3.2.1 XRD analysis of AS

The crystallographic structure of the sample was evaluated using XRD to get additional insight into the development of the AS moiety and to determine if the sample was in an amorphous or crystalline phase. The diffraction patterns in Figure 26 (a) show that the sample was amorphous in structure and the peak at an angle in the 20–35° range, which can be attributed to the presence of amorphous silica and AS [84]. Figure 26 (b) shows the XRD pattern of AC produced from "brown algae," with peaks at angles of 23° indicating carbonaceous structure. The presence of a very small peak at an angle 15° indicates the presence of phosphor because H_3PO_4 was used as an activated agent [67].

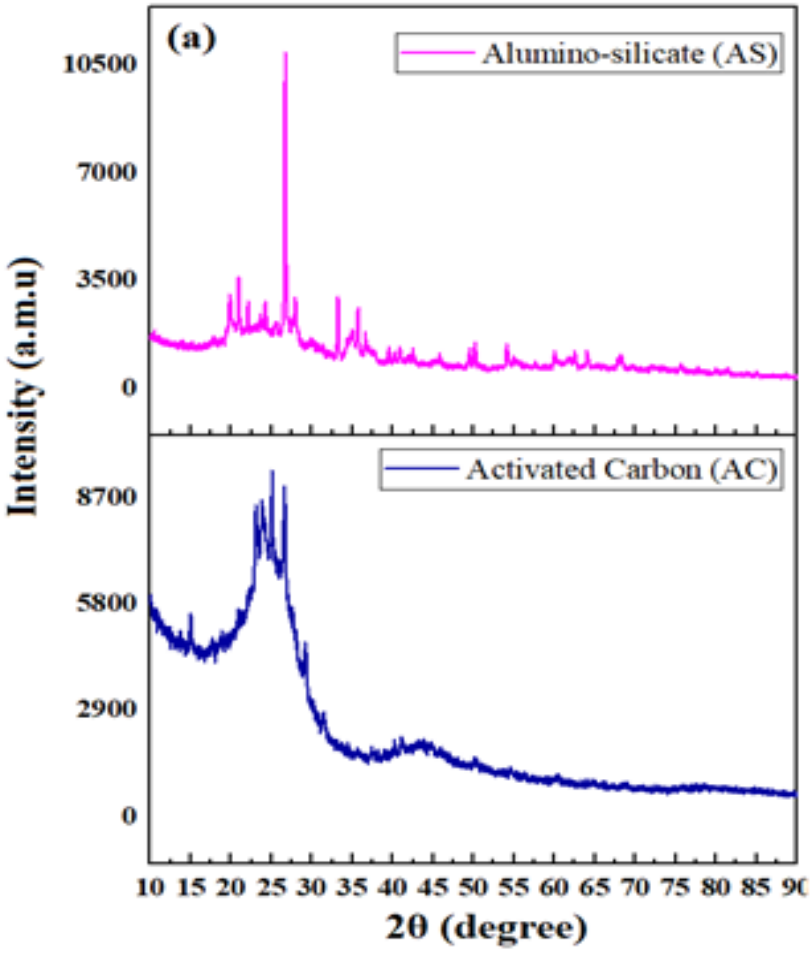

Figure 26. XRD analysis of AS (a) and AC (b)

3.2.2 SEM analysis of AS

The scanning electron microscopy image in Figure 27 (a) shows the AC prepared from the brown algae has a variety of shapes. Figure 27 (b) shows the SEM images of AS, it reveals that small pores are formed when $ZnCl_2$ is used as a chemical activation agent to make them.

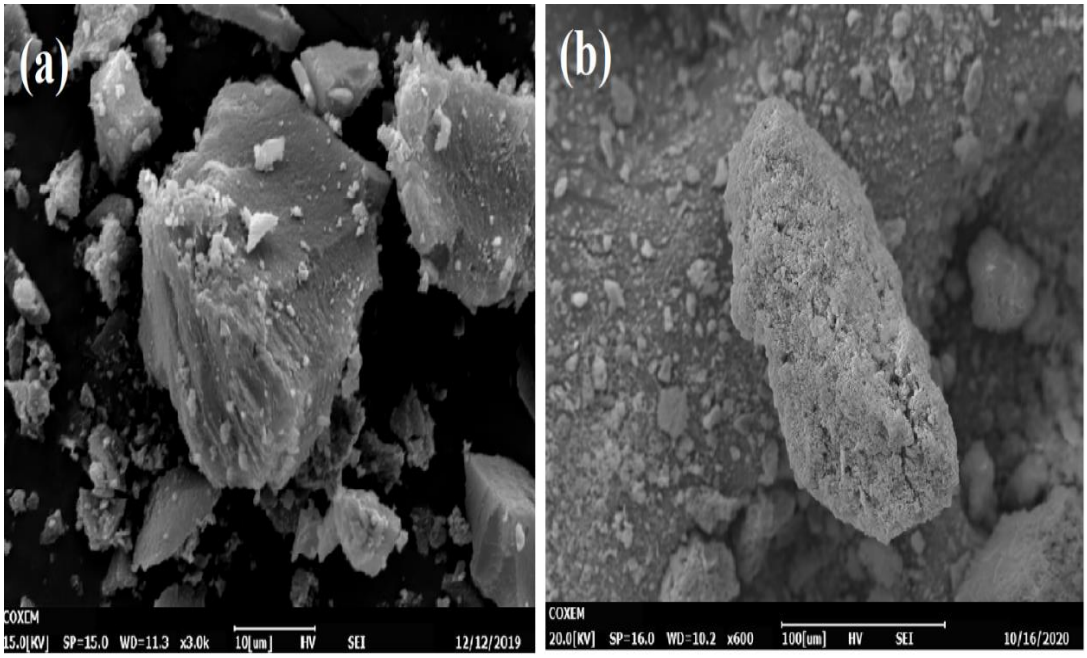

Figure 27. SEM image of AC (a) and AS (b)

3.2.3 BET analysis of AS

The BET surface area of prepared AS was 943 m^2g^{-1}. In general, the BET surface area of the AS was in the range of 510-970 m^2g^{-1} [52].

3.3 Membrane characterization

3.3.1 XRD analysis of membrane (ZIF-AC-AS)

Figure 28 shows the XRD peaks of ZIF and ZIF has a typical peak at 7.26°, 12.66°, 16.41°, and 17.95°. The peak at an angle 7.26° indicates ZIF-8 has a crystallinity structure. Small peaks at angles 60-68° suggest effective ZIF impregnation on Al_2O_3 [85]. The effective aperture size of ZIF is 3.6–3.8 Å, slightly bigger than the 3.4 Å reported from single-crystal XRD [86]. As seen in the image, adding carbon weakens the distinctive peaks. Normally, reduced crystallinity aids particle dispersion in the polymer-based matrix [87].

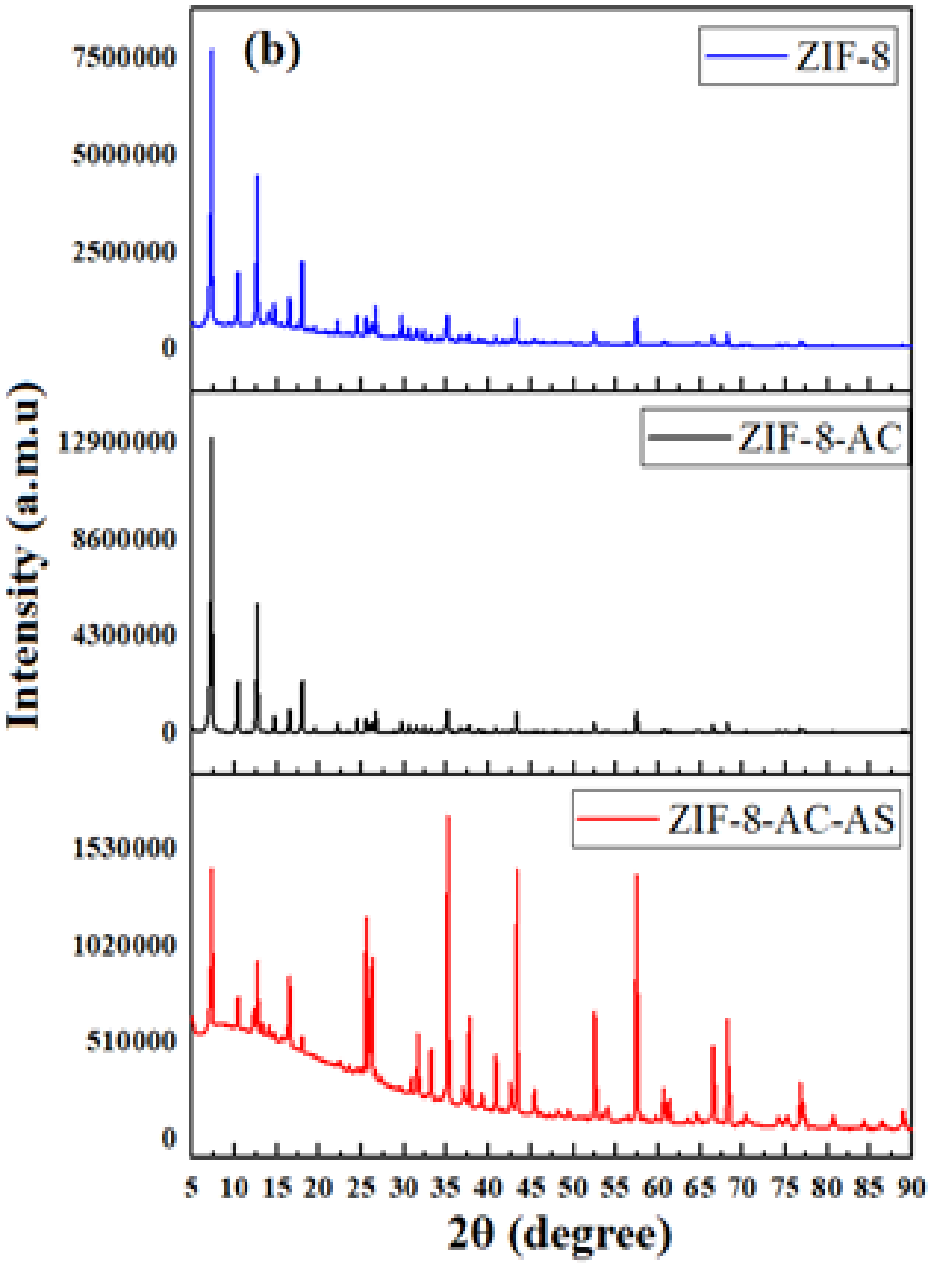

Figure 28. XRD analysis of ZIF (a), ZIF-AC (b) and ZIF-AC-AS (c)

3.3.2 SEM analysis of membrane (ZIF-AC-AS)

Figure 29 (a & b) show the SEM image of ZIF particles in the prepared membrane. Figure 30 shows the ZIF particle shape and the shape of the ZIF particle (in Figure 30 (a)) was shown as a hexagonal shape. The incorporation of AC and AS increased the membrane's overall mechanical strength. Figures 30 (a & b) revealed that AC and AS particles were incorporated with ZIF particles. Figure 31 shows the morphology of ZIF (a) and ZIF-AC-AS (b) membranes. Figures 32 (a & b) show the cross-section images of the prepared ZIF-AC-AS membrane.

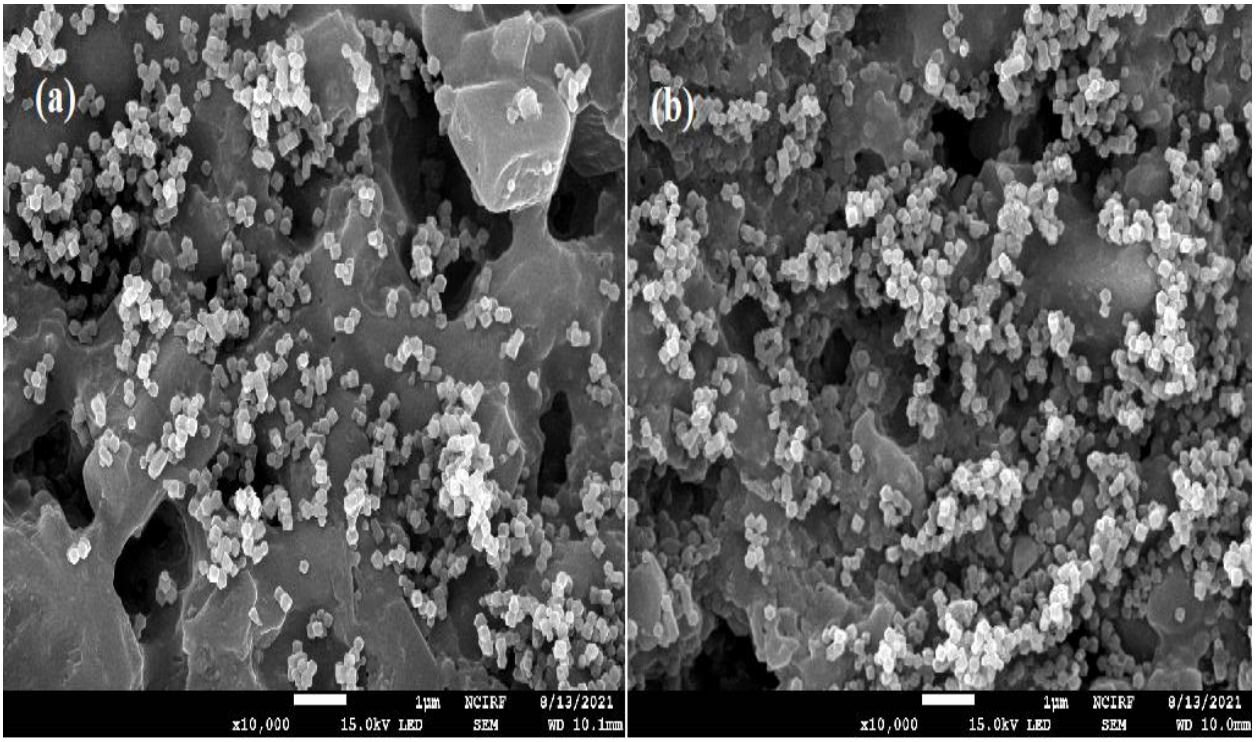

Figure 29. SEM image of ZIF

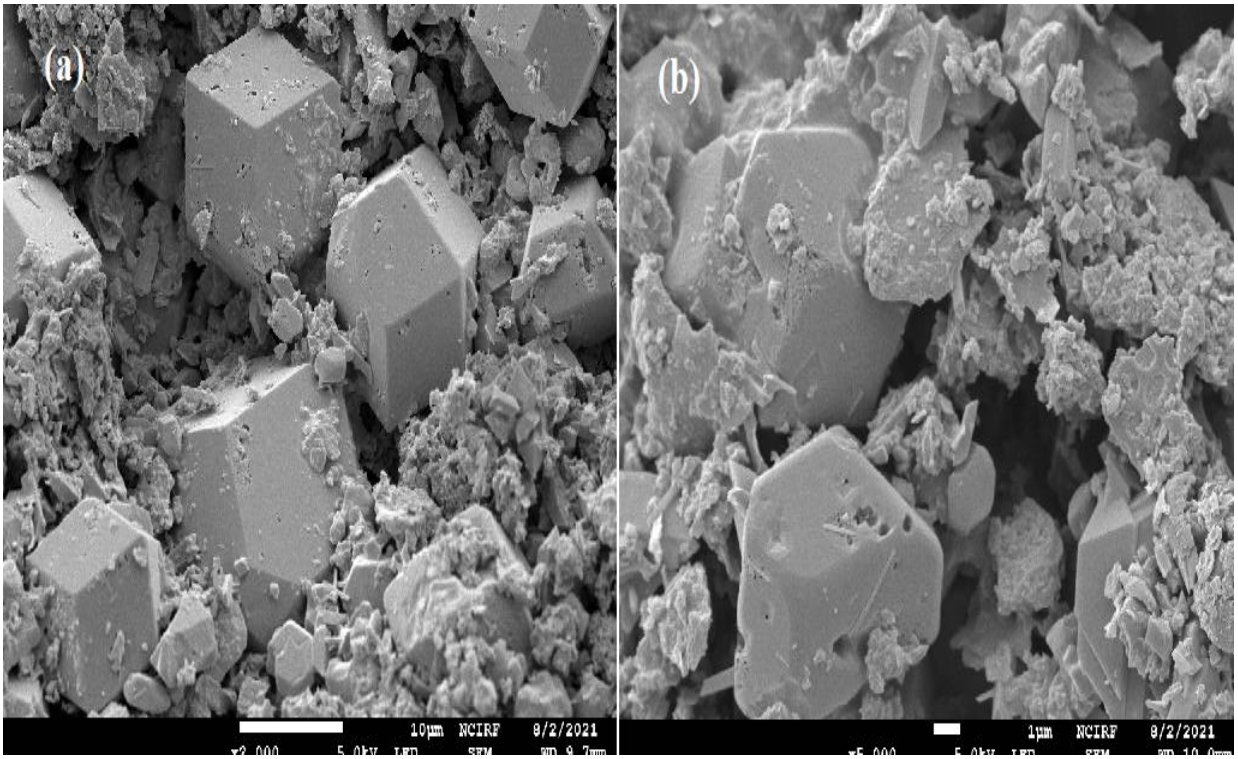

Figure 30. SEM image of ZIF-AC-AS

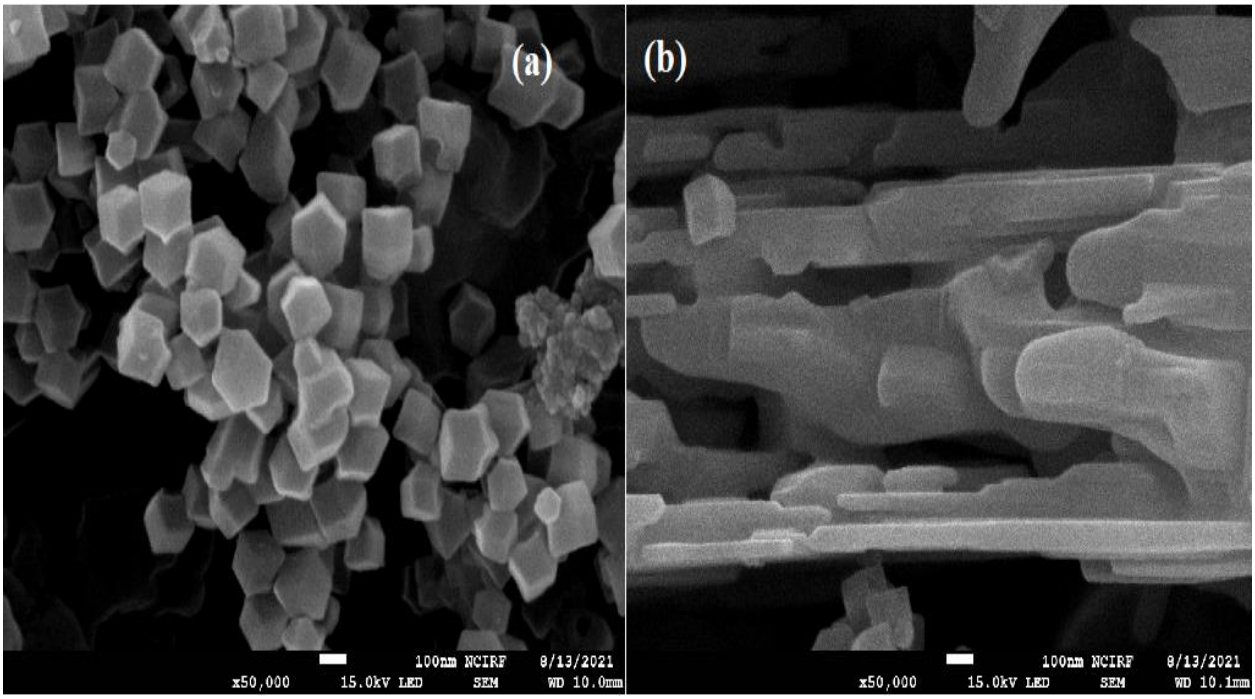

Figure 31. SEM image of ZIF (a) and ZIF-AC-AS (b)

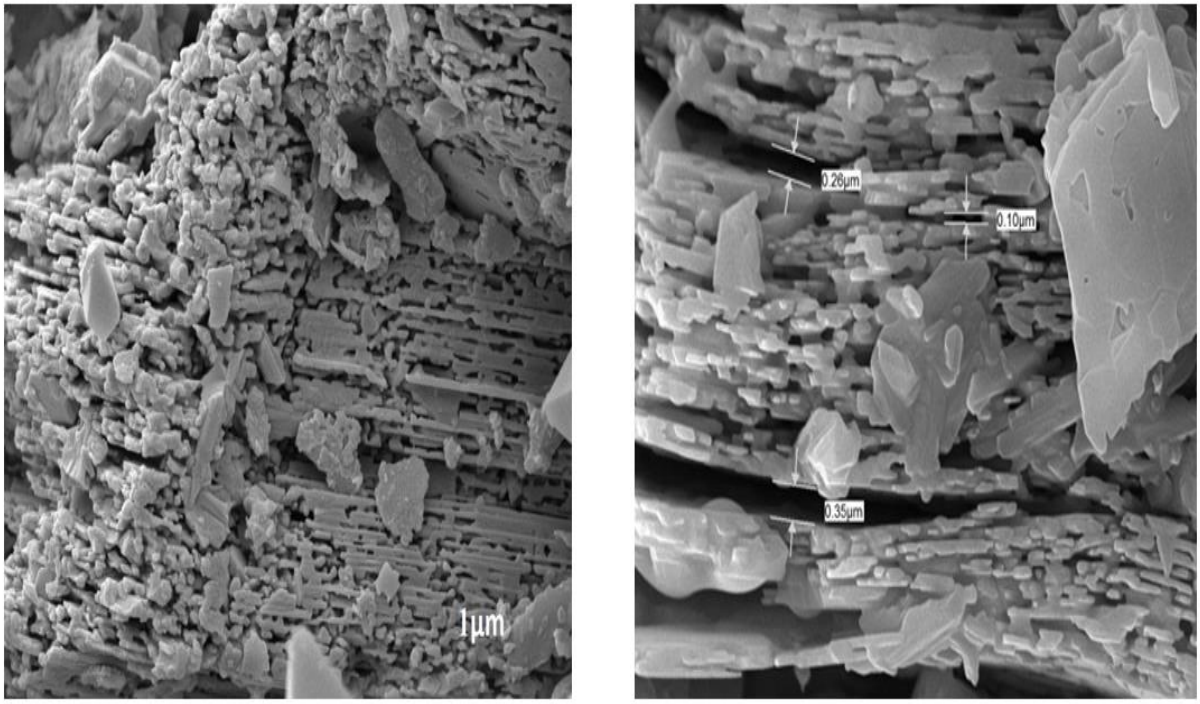

Figure 32. SEM Cross-section image of ZIF-AC-AS

3.3.3 EDX analysis of membrane (ZIF-AC-AS)

The AC prepared from algae biomass revealed that the carbon content was 85 %, but a small amount of phosphorus still existed because H_3PO_4 was used to activate the AC. According to the literature, the presence of phosphorus in the activated samples is due to the lowest evaporation point of phosphorus derivate at 350 °C. Table 6 shows the EDX elemental composition of AC, AS, and ZIF-alumina silicate-based membranes. The AS exhibited a Si content of 41%, oxygen of 37%, and aluminum of 15%.

Table 6. EDX elemental analysis of ZIF-AC-AS membrane

Sample ID	EDX elemental Analysis (Composition%)									
	C	P	N	O	Na	Zn	Al	Si	Cl	Fe
AC	85	15	—	—	—	—	—	—	—	—
AS	—	—	—	37	—	—	15	42		7
ZIF	47	—	15	4	2	21	—	—	11	—
ZIF-AC	39	—	18	17	2	16	—	—	—	—
ZIF-AC-AS	28	—	6	30	0	3	33	—	—	—

AC= Activated carbon AS= Aluminosilicate

The permeance π_i for the component i is defined by the below equation.

$$\pi_i = \frac{J_i}{\Delta P_i}$$

Where ΔP_i is the partial pressure difference of a component i through the membrane and J_i is the flux for the component. The flux for a component i is defined by the equation below.

$$J_i = \frac{F_i}{A}$$

Where A is the area of the membrane used for the gas separation. The area of the membrane is defined by the equation below.

$$A = \frac{d^2\pi}{4}$$

Where F_i (mol s^{-1}) is the permeate molar flow rate of the component i through the membrane. Because the experiments are carried out at room temperature and 100 °C, the value of T is 273 K and 373 K, respectively [88].

$$F_i = n = \frac{PV}{RT}$$

For the permeability calculations, the value of the flow rate was taken from the mass flow controller (MFC). When the experiment is completed the installed software automatically generates the excel files. The membrane area was explained in the experimental section. Figures 33 to 36 show the flow rate versus time graphs relationship. Table 7 shows the permeability of the ZIF and ZIF-AC-AS membranes. Figures 37 and 38 show the gas chromatography results for the mixture of gases. Figure 37 reveals that the permeate gas contains a higher composition of CH_4 (42%) and Figure 38 reveals that the H_2 has the highest permeate composition in the permeate sample.

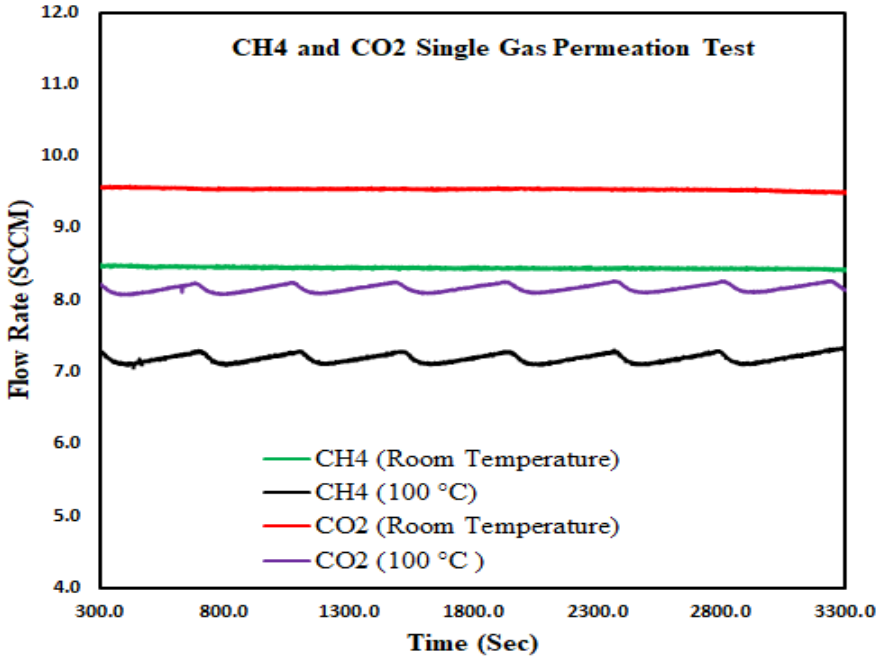

Figure 33. Single gas permeation test for CH_4 and CO_2 gases

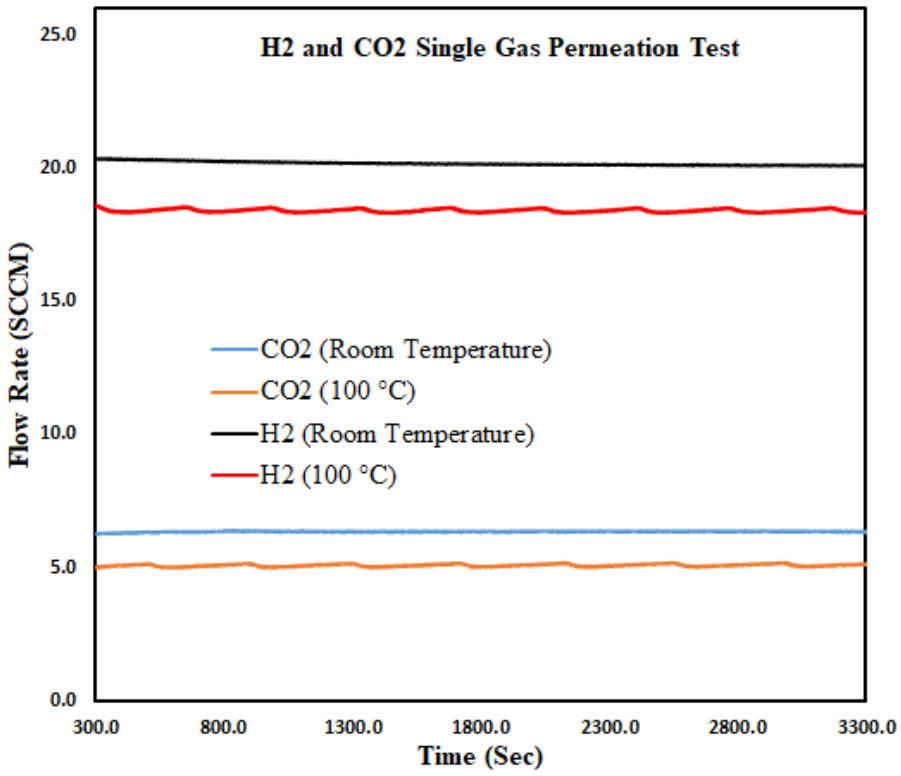

Figure 34. Mixture of gas permeation test for CH_4 and CO_2 gases

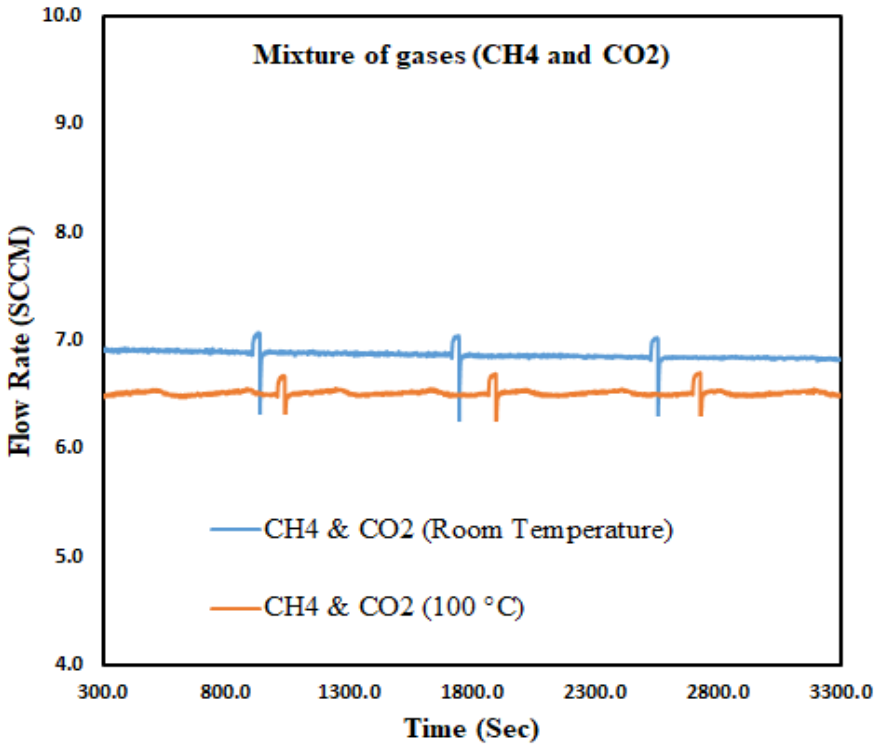

Figure 35. Single gas permeation test for H_2 and CO_2 gases

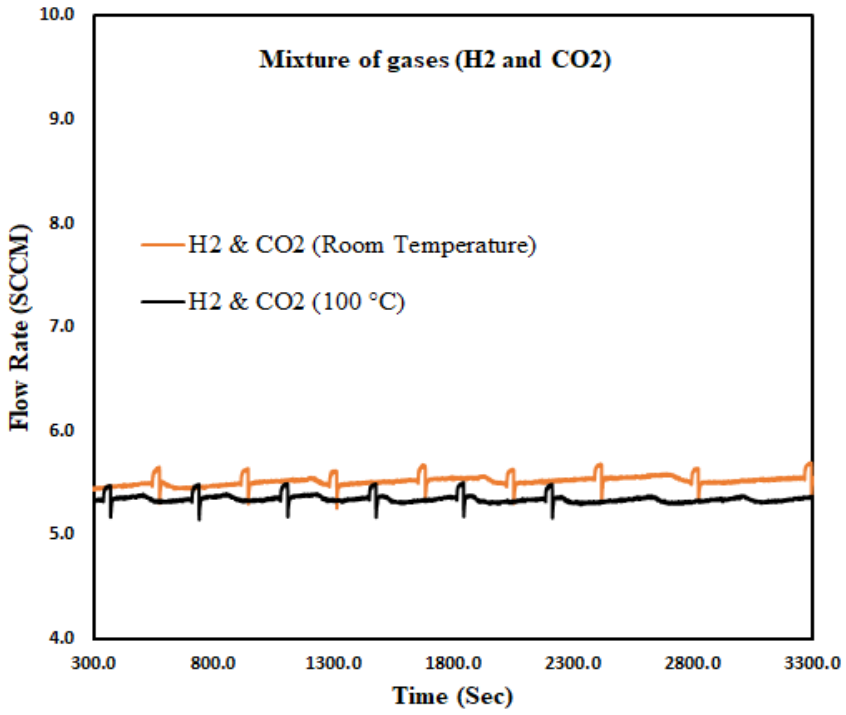

Figure 36. Mixture of gas permeation test for H_2 and CO_2 gases

Table 7 Gas permeability of ZIF-8 and ZIF-AC-AS membrane

Membrane Type	Gases Permeability (Barrer)					Selectivity	Temperature	References
	H_2	CO_2	CH_4	H_2 & CO_2	CH_4 & CO_2		(°C)	
ZIF-8	233.13							[51]
	180.29	39.70	14.32			4.5 (H_2/CO_2)	22	[89]
	245.67		18.80			13.0(H_2/CH_4)		
			33.43					[90]
			18.59					
ODPA-TMPDA/5% GO + 10% ZIF-8		14.65	0.35		90.74		25	[91]
ZIF-8	3164.17	156.11		134.62		20.2(H_2/CO_2)	25	This Study
	361.19	99.70		104.77		3.4 (H_2/CO_2)	100	This Study
ZIF-AC-AS		232.23	207.46		168.95	1.1(CO_2/CH_4)	25	This Study
		203.58	146.86		130.44	1.3 (CO_2/CH_4)	100	This Study

1 Barrer= $3.35*10^{-16}$ $\frac{mol.m}{m^2.s.Pa}$

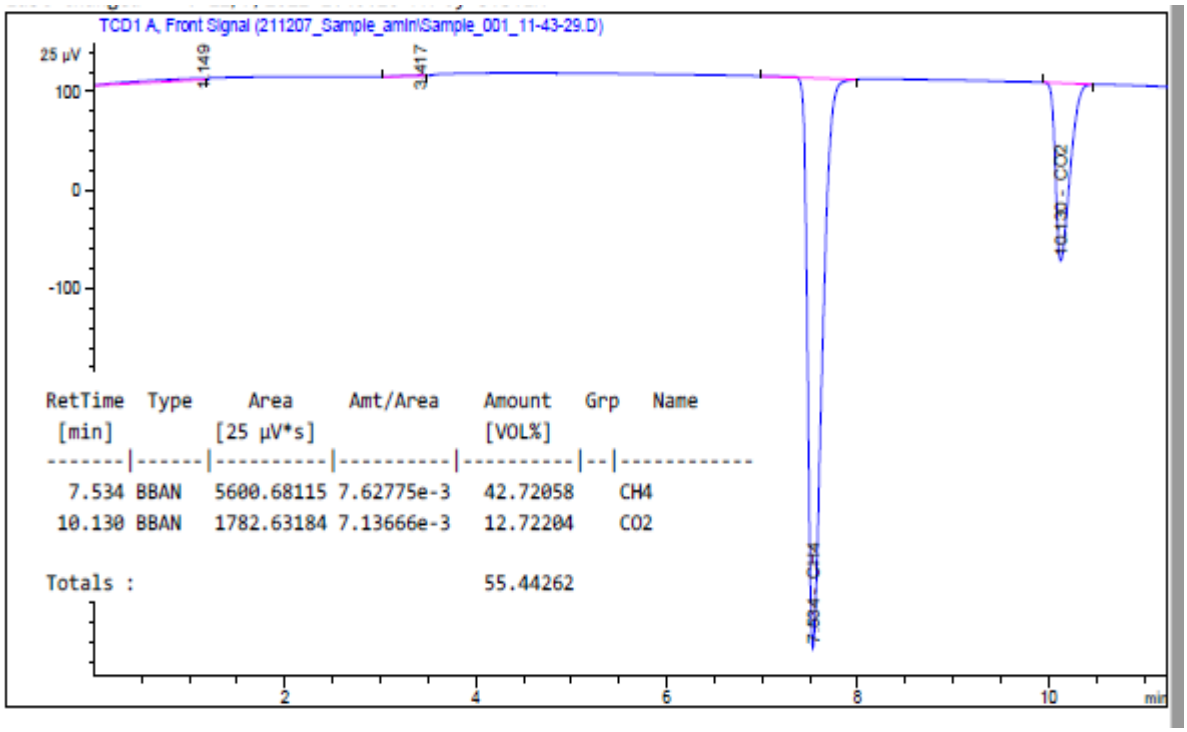

Figure 37. Gas chromatography results for CH_4 and CO_2 gases mixture

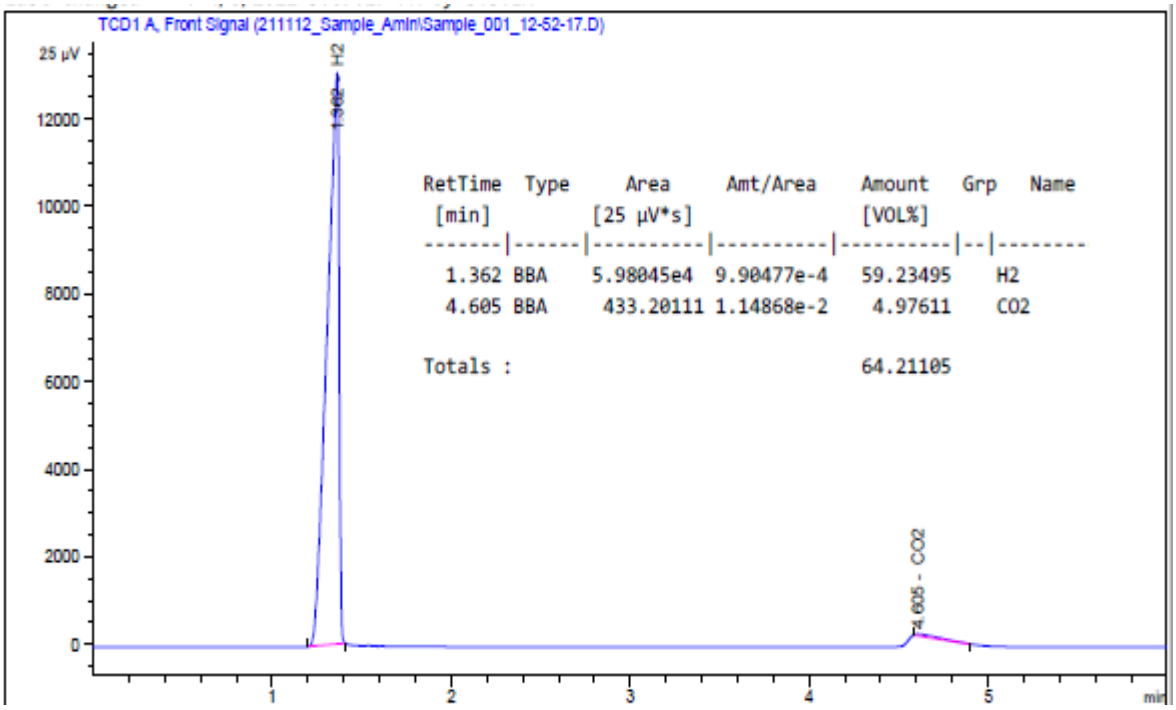

Figure 38. Gas chromatography results for H_2 and CO_2 gases mixture

AS is a type of zeolite and zeolite-based membranes are attracted and have the potential to separate the gases from chemical synthesis [92]. In particular, the inorganic AS coordinates with the metal ions into the regular framework. The diverse structure of ZIF is similar to that of conventional AS zeolites. Typically, Zn^{2+} ions play the role of silicon and the imidazolate anions form bridges that mimic the role of oxygen in zeolites with the metal–imidazole–metal [93].

In addition, the incorporation of AS into the ZIF helps to control the porosity and crystal size of the ZIF [94]. Now the question comes to mind: why was the AC added to the prepared membrane? In this research, AS is not directly purchased from the market. It is made from a natural resource (algae). When the mixing of ZIF and AS (algae-based) was performed, proper homogeneous mixing was not done (Please see figure 17 (b)). Then AC was added to the ZIF-AS solution. It was added in a very small amount (1.7%). After adding the AC, the mixing was fine and no particles agglomerated (Please see figure 17 (a)). In this research, the addition of a small amount of AC acts as an additive material.

Chapter 4. Conclusions

In this study, the zeolitic imidazolate framework membrane was incorporated with AC and AS. The prepared membranes were used for the separation of gases such as hydrogen methane and carbon dioxide gas.

The AC prepared from brown algae exhibited a carbon content of 85%. The surface area of the AS was 943 m^2g^{-1}. Due to the creation of ZIF crystals with an AC and AS particle, the surface of the membrane was uneven and bumpy (see Appendix). This uneven and bumpy surface would allow the gases to permeate through the developed channels. The permeation test results from the ZIF membrane revealed the permeation value of H_2 and CO_2 were 3164.17, 156.11 (Barrer), respectively, at room temperature. The permeation test results from the ZIF-AC-AS membrane revealed that the permeation value of CH_4 and CO_2 were 207.46, 232.23 (Barrer), respectively, at room temperature. As the temperature increased from room temperature to 100 °C, the permeation values of CH_4 and CO_2 decreased slightly to 146.86 and 203.58 (Barrer), respectively. Therefore, this study showed that small incorporations of AC and AS in the ZIF structure increased the gas permeability.

For future studies, the prepared membrane can be used at higher temperatures because the concentration of aluminum in the membrane composition would make the membrane more stable and effective for gas separation at higher temperatures. The gases having greater kinetic diameters, such as propane and propylene, can be tested. In order to obtain the higher purity of gases, the installed lab scale system needs to be modified according to the cyclic system.

Appendices

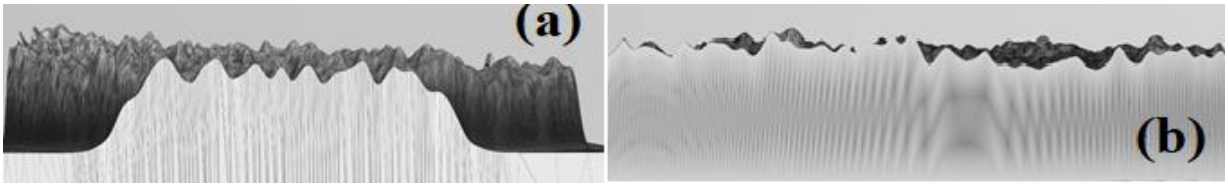

Figure A1. Al_2O_3 disc position during autoclave reaction

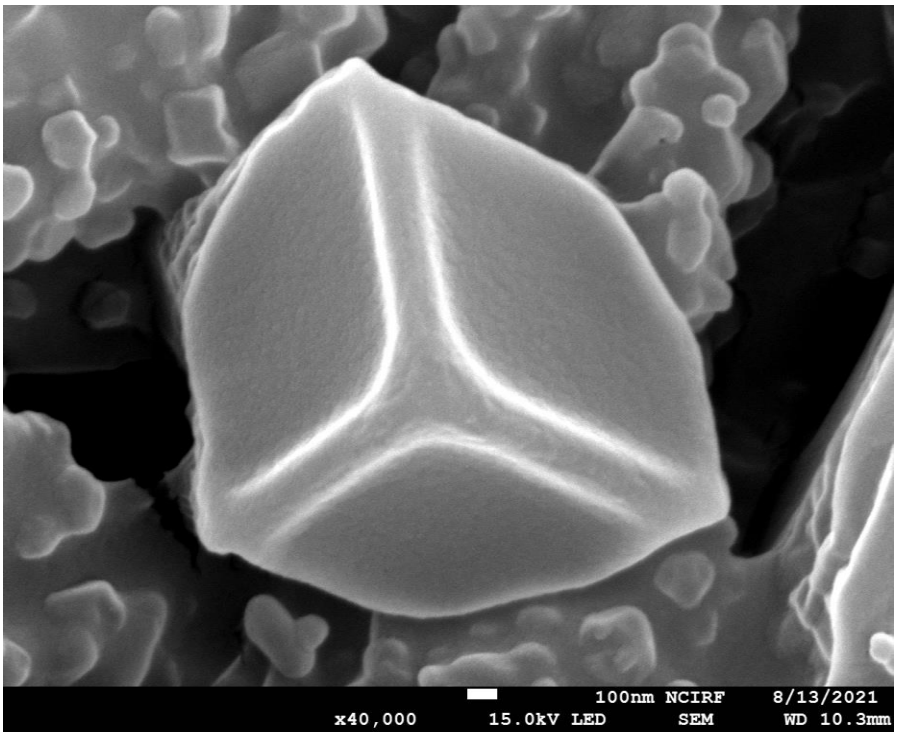

Figure A2. ZIF particle hexagonal shape

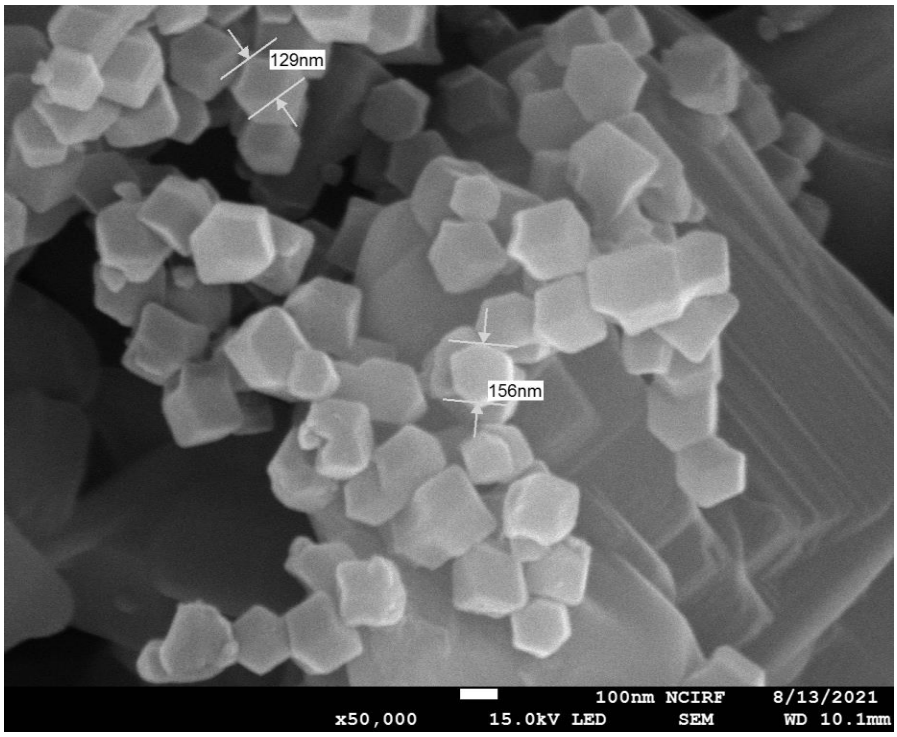

Figure A3. ZIF particles size

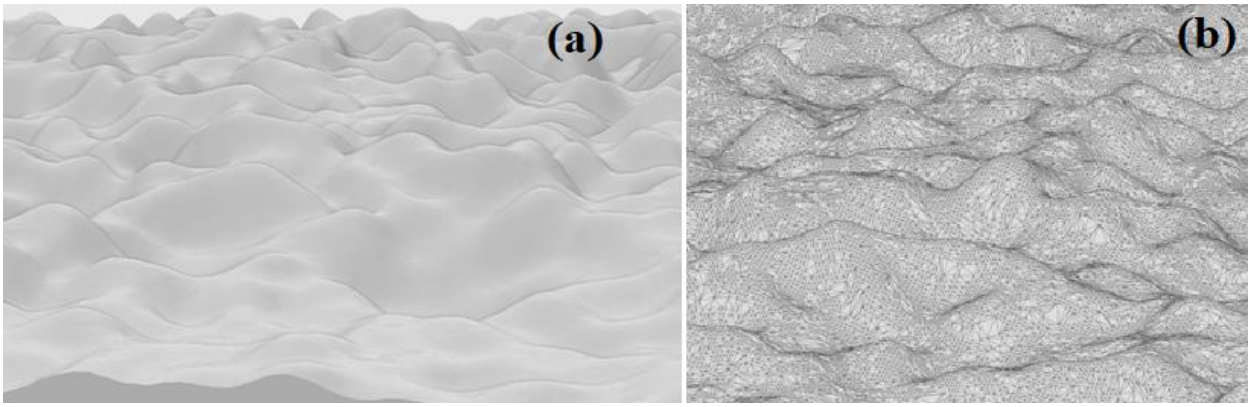

Figure A4. Membrane surface analysis

Electron Image 1

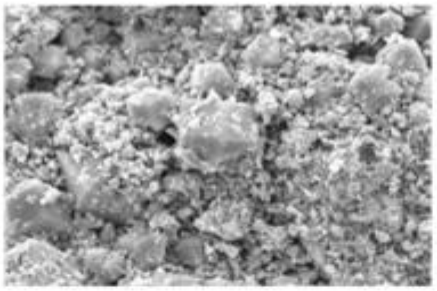

EDS Layered Image 1

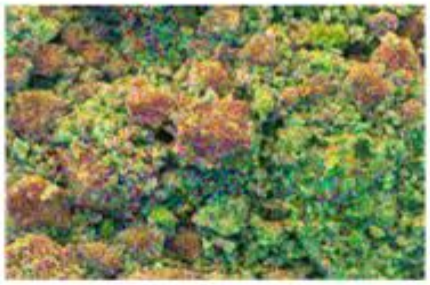

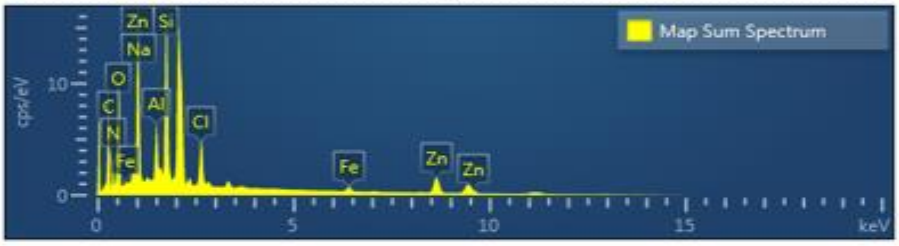

Element	Line Type	Apparent Concentration	k Ratio	Wt%	Wt% Sigma	Atomic %	Standard Label	Factory Standard	Standard Calibration Date
C	K series	3.21	0.03213	35.24	0.29	48.58	C Vit	Yes	
N	K series	5.07	0.00903	14.33	0.36	16.94	BN	Yes	
O	K series	6.59	0.02218	22.10	0.20	22.86	SiO2	Yes	
Na	K series	1.24	0.00524	1.99	0.07	1.43	Albite	Yes	
Al	K series	1.38	0.00989	2.26	0.03	1.39	Al2O3	Yes	
Si	K	4.14	0.0328	6.26	0.05	3.69	SiO2	Yes	

	series		4						
Cl	K series	1.68	0.01471	2.54	0.03	1.19	NaCl	Yes	
Fe	K series	0.80	0.00802	1.28	0.06	0.38	Fe	Yes	
Zn	L series	4.85	0.04853	14.00	0.14	3.55	Zn	Yes	
Total:				100.00		100.00			

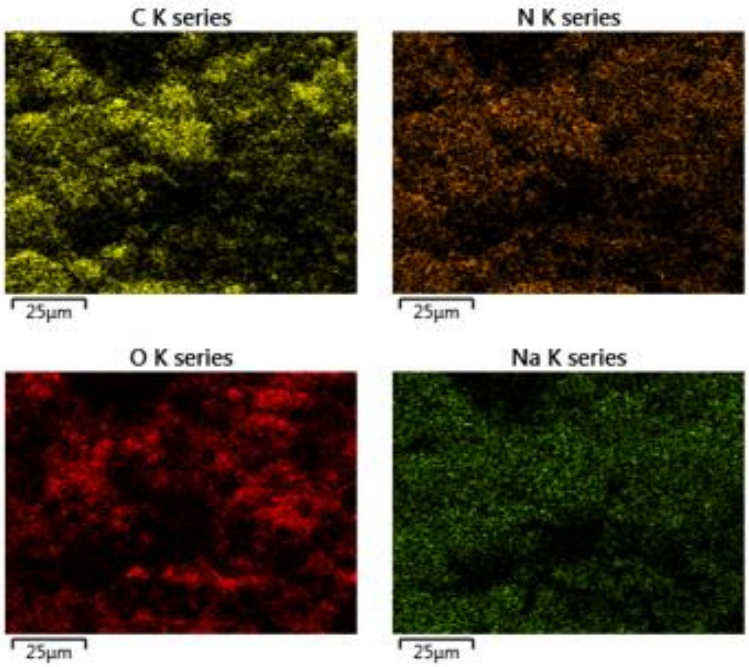

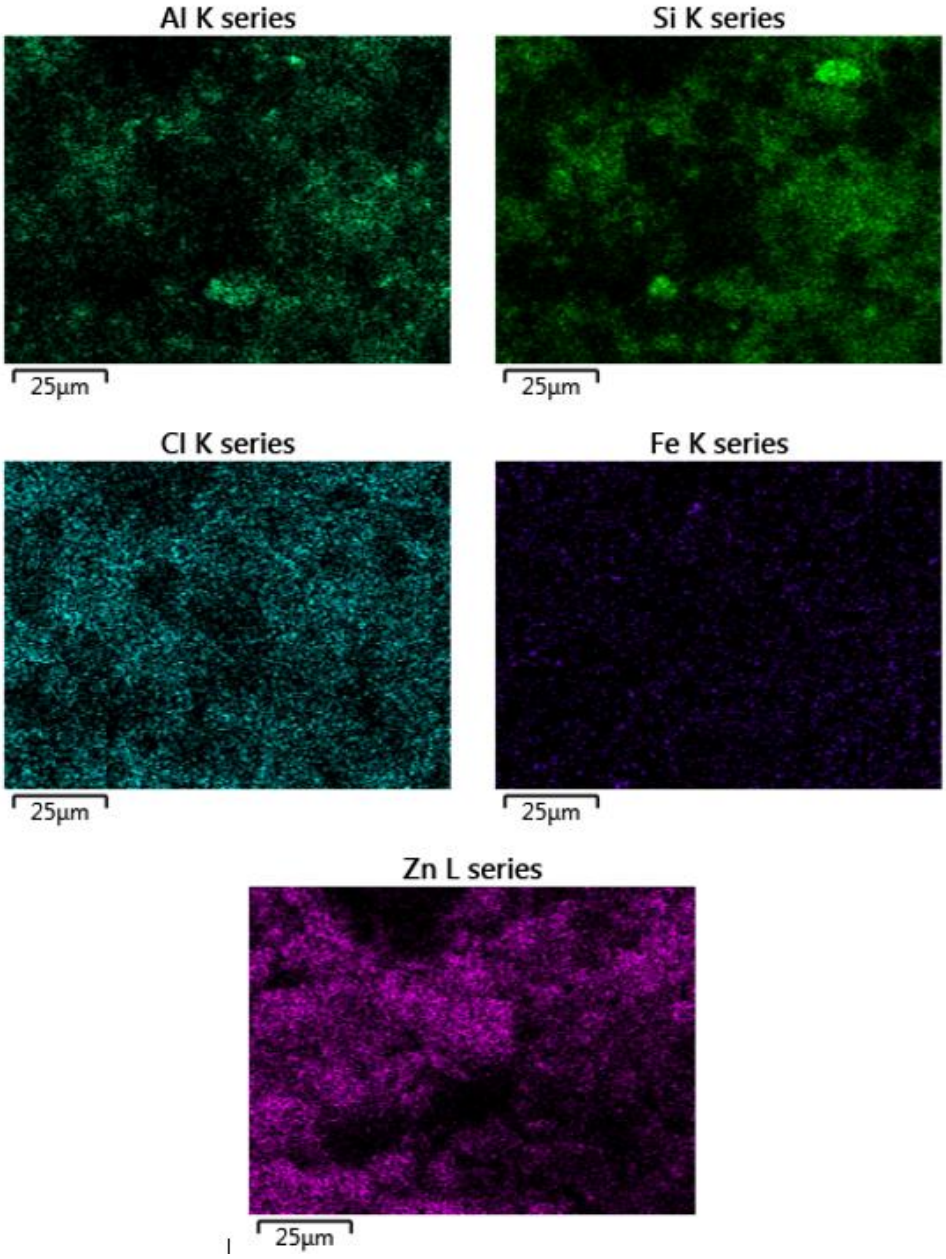

Figure A5. EDX Zn mapping for ZIF-AC-AS membrane

Figure A6. Steps Involved for the conversion of biomass into AC

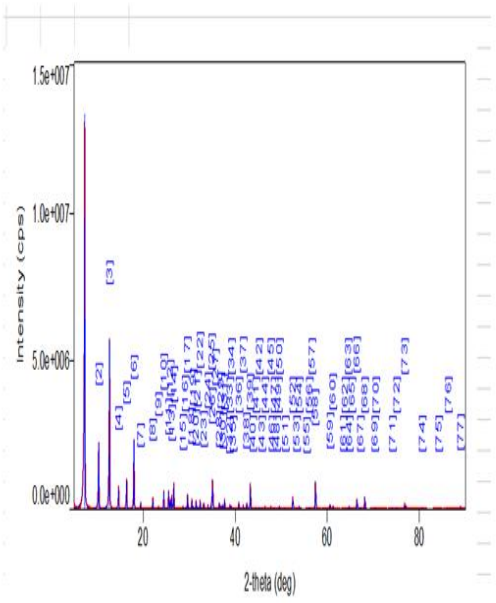

1	7.3000(19)	13353813(3898)	ZIF-8, activated, Basolite Z1200T(1,1,0)
2	10.3600(1	2273900(1616)	ZIF-8, activated, Basolite Z1200T(2,0,0)
3	12.700(3)	5709736(2566)	ZIF-8, activated, Basolite Z1200T(2,1,1)
4	14.680(3)	768142(951)	ZIF-8, activated, Basolite Z1200T(2,2,0),Sodium Hydrogen Carbonate Oxide(1,2,0)
5	16.4200(1	997108(1086)	ZIF-8, activated, Basolite Z1200T(3,1,0)
6	18.020(2)	2325200(1662)	ZIF-8, activated, Basolite Z1200T(2,2,2)
7	19.480(5)	215346(514)	ZIF-8, activated, Basolite Z1200T(3,2,1),Sodium Hydrogen Carbonate Oxide(2,0,0)
8	22.1200(1	385608(689)	ZIF-8, activated, Basolite Z1200T(4,1,1)
9	23.340(17	57573(269)	ZIF-8, activated, Basolite Z1200T(4,2,0),Sodium Hydrogen Carbonate Oxide(1,3,1)
10	24.5000(1	605976(880)	ZIF-8, activated, Basolite Z1200T(3,3,2)
11	25.540(4)	598620(866)	ZIF-8, activated, Basolite Z1200T(4,2,2)
12	25.920(4)	249282(571)	Zinc Nitrate Hydrate(2,-1,1),Natroxalate, syn(1,0,0)

Figure A7. Prepared membrane chemical compounds

References

[1] J. M. Schopf, “James m. schopf,” pp. 521–527.

[2] X. Liu *et al.*, “Review of the characteristics and graded utilisation of coal gasification slag,” *Chinese J. Chem. Eng.*, vol. 35, pp. 92–106, 2021, doi: 10.1016/j.cjche.2021.05.007.

[3] A. Midilli, H. Kucuk, M. E. Topal, U. Akbulut, and I. Dincer, “A comprehensive review on hydrogen production from coal gasification: Challenges and Opportunities,” *Int. J. Hydrogen Energy*, vol. 46, no. 50, pp. 25385–25412, 2021, doi: 10.1016/j.ijhydene.2021.05.088.

[4] J. G. Speight, “Gasification Processes,” *Handb. Pet. Refin.*, no. October, pp. 611–654, 2020, doi: 10.1201/9781315374079-22.

[5] Y. Shen, Y. Hu, M. Wang, W. Bao, L. Chang, and K. Xie, “Speciation and thermal transformation of sulfur forms in high-sulfur coal and its utilization in coal-blending coking process: A review,” *Chinese J. Chem. Eng.*, vol. 35, pp. 70–82, 2021, doi: 10.1016/j.cjche.2021.04.007.

[6] S. R. Hamedani, M. Villarini, A. Colantoni, M. Moretti, and E. Bocci, “Life cycle performance of hydrogen production via agro-industrial residue gasification-a small scale power plant study,” *Energies*, vol. 11, no. 3, 2018, doi: 10.3390/en11030675.

[7] “Syngas production by plasma gasification,” WO2012/064936 A1, 2012.

[8] Z. Du *et al.*, “A review of hydrogen purification technologies for fuel cell vehicles,” *Catalysts*, vol. 11, no. 3, pp. 1–19, 2021, doi: 10.3390/catal11030393.

[9] H. P. Kirchner, “Potential Applications,” *Strength. Ceram.*, pp. 229–236, 2020, doi: 10.1201/9781498710466-9.

[10] N. Pal and M. Agarwal, “Advances in materials process and separation mechanism of the membrane towards hydrogen separation,” *Int. J. Hydrogen Energy*, vol. 46, no. 53, pp.

27062–27087, 2021, doi: 10.1016/j.ijhydene.2021.05.175.

[11] J. Shang *et al.*, “Separation of CO2and CH4by Pressure Swing Adsorption Using a Molecular Trapdoor Chabazite Adsorbent for Natural Gas Purification,” *Ind. Eng. Chem. Res.*, vol. 59, no. 16, pp. 7857–7865, 2020, doi: 10.1021/acs.iecr.0c00317.

[12] A. Mivechian and M. Pakizeh, “Hydrogen recovery from Tehran refinery off-gas using pressure swing adsorption, gas absorption and membrane separation technologies: Simulation and economic evaluation,” *Korean J. Chem. Eng.*, vol. 30, no. 4, pp. 937–948, 2013, doi: 10.1007/s11814-012-0221-y.

[13] J. Godin, W. Liu, S. Ren, and C. C. Xu, “Advances in recovery and utilization of carbon dioxide: A brief review,” *J. Environ. Chem. Eng.*, vol. 9, no. 4, p. 105644, 2021, doi: 10.1016/j.jece.2021.105644.

[14] H. Oh and M. Hirscher, “Quantum Sieving for Separation of Hydrogen Isotopes Using MOFs,” *Eur. J. Inorg. Chem.*, vol. 2016, no. 27, pp. 4278–4289, 2016, doi: 10.1002/ejic.201600253.

[15] J. C. Davis, R. J. Valus, R. Eshraghi, and A. E. Velikoff, “Facilitated transport membrane hybrid systems for olefin purification,” *Sep. Sci. Technol.*, vol. 28, no. 1–3, pp. 463–476, 1993, doi: 10.1080/01496399308019500.

[16] Y. Taniguchi and M. Ishida, “Hydrogen purification method from reformed gas containing high concentration of CO by using metal hydride,” *IEEJ Trans. Power Energy*, vol. 126, no. 12, pp. 1267–1274, 2006, doi: 10.1541/ieejpes.126.1267.

[17] S. Elhenawy, M. Khraisheh, F. AlMomani, and M. Hassan, “Key applications and potential limitations of ionic liquid membranes in the gas separation process of CO2, CH4, N2, H2 or mixtures of these gases from various gas streams,” *Molecules*, vol. 25, no. 18, 2020, doi: 10.3390/molecules25184274.

[18] H. Chen, D. Cai, C. Chen, J. Wang, P. Qin, and T. Tan, “Novel distillation process for effective and stable separation of high-concentration acetone-butanol-ethanol mixture from fermentation-pervaporation integration process,” *Biotechnol. Biofuels*, vol. 11, no. 1,

pp. 1–13, 2018, doi: 10.1186/s13068-018-1284-8.

[19] P. Bernardo, E. Drioli, and G. Golemme, “Membrane gas separation: A review/state of the art,” *Ind. Eng. Chem. Res.*, vol. 48, no. 10, pp. 4638–4663, 2009, doi: 10.1021/ie8019032.

[20] R. Lin, B. Villacorta Hernandez, L. Ge, and Z. Zhu, “Metal organic framework based mixed matrix membranes: An overview on filler/polymer interfaces,” *J. Mater. Chem. A*, vol. 6, no. 2, pp. 293–312, 2018, doi: 10.1039/c7ta07294e.

[21] M. Achparaki *et al.*, “We are IntechOpen , the world ’ s leading publisher of Open Access books Built by scientists , for scientists TOP 1 %,” *Intech*, p. 13, 2012, [Online]. Available: http://dx.doi.org/10.1039/C7RA00172J%0Ahttps://www.intechopen.com/books/advanced-biometric-technologies/liveness-detection-in-biometrics%0Ahttp://dx.doi.org/10.1016/j.colsurfa.2011.12.014.

[22] Z. Huang *et al.*, “Diffusion behavior of gas molecules in the one-dimensional channel of AlPO4-5 molecular sieves,” *Microporous Mesoporous Mater.*, vol. 340, no. March, p. 112024, 2022, doi: 10.1016/j.micromeso.2022.112024.

[23] Y. Zhang, Y. Jia, M. Li, and L. Hou, “Influence of the 2-methylimidazole/zinc nitrate hexahydrate molar ratio on the synthesis of zeolitic imidazolate framework-8 crystals at room temperature,” *Sci. Rep.*, vol. 8, no. 1, pp. 1–8, 2018, doi: 10.1038/s41598-018-28015-7.

[24] N. W. Ockwig and T. M. Nenoff, “Membranes for hydrogen separation,” *Chem. Rev.*, vol. 107, no. 10, pp. 4078–4110, 2007, doi: 10.1021/cr0501792.

[25] Y. Song, M. He, J. Zhao, and W. Jin, “Structural manipulation of ZIF-8-based membranes for high-efficiency molecular separation,” *Sep. Purif. Technol.*, vol. 270, no. January, p. 118722, 2021, doi: 10.1016/j.seppur.2021.118722.

[26] X. Jiang, S. Li, Y. Bai, and L. Shao, “Ultra-facile aqueous synthesis of nanoporous zeolitic imidazolate framework membranes for hydrogen purification and olefin/paraffin separation,” *J. Mater. Chem. A*, vol. 7, no. 18, pp. 10898–10904, 2019, doi:

10.1039/c8ta11748a.

[27] E. F. Krivoshapkina, P. V. Krivoshapkin, and A. A. Vedyagin, “Synthesis of Al2O3–SiO2–MgO ceramics with hierarchical porous structure,” *J. Adv. Ceram.*, vol. 6, no. 1, pp. 11–19, 2017, doi: 10.1007/s40145-016-0210-4.

[28] R. Bedard and C. Liu, “Recent Advances in Zeolitic Membranes,” *Annu. Rev. Mater. Res.*, vol. 48, pp. 83–110, 2018, doi: 10.1146/annurev-matsci-070317-124605.

[29] H. T. Lu, W. Li, E. S. Miandoab, S. Kanehashi, and G. Hu, “The opportunity of membrane technology for hydrogen purification in the power to hydrogen (P2H) roadmap: a review,” *Front. Chem. Sci. Eng.*, vol. 15, no. 3, pp. 464–482, 2021, doi: 10.1007/s11705-020-1983-0.

[30] J. van den Bergh, W. Zhu, J. Gascon, J. A. Moulijn, and F. Kapteijn, “Separation and permeation characteristics of a DD3R zeolite membrane,” *J. Memb. Sci.*, vol. 316, no. 1–2, pp. 35–45, 2008, doi: 10.1016/j.memsci.2007.12.051.

[31] P. Du *et al.*, “Efficient scale-up synthesis and hydrogen separation of hollow fiber DD3R zeolite membranes,” *J. Memb. Sci.*, vol. 636, no. June, p. 119546, 2021, doi: 10.1016/j.memsci.2021.119546.

[32] X. Gao, C. Da, C. Chen, Z. Li, X. Gu, and S. K. Bhatia, “The induced orientation effect of linear gases during transport in a NaA zeolite membrane modified by alkali lignin,” *J. Memb. Sci.*, vol. 620, no. August 2020, p. 118971, 2021, doi: 10.1016/j.memsci.2020.118971.

[33] J. Xu, K. G. Haw, Z. Li, S. Pati, Z. Wang, and S. Kawi, “A mini-review on recent developments in SAPO-34 zeolite membranes and membrane reactors,” *React. Chem. Eng.*, vol. 6, no. 1, pp. 52–66, 2021, doi: 10.1039/d0re00349b.

[34] W. Ouyang *et al.*, “Dynamic ammonia adsorption by FAU zeolites to below 0.1 ppm for hydrogen energy applications,” *Int. J. Hydrogen Energy*, vol. 46, no. 64, pp. 32559–32569, 2021, doi: 10.1016/j.ijhydene.2021.07.107.

[35] H. Wang, X. Dong, and Y. S. Lin, “Highly stable bilayer MFI zeolite membranes for high temperature hydrogen separation,” *J. Memb. Sci.*, vol. 450, pp. 425–432, 2014, doi: 10.1016/j.memsci.2013.08.030.

[36] H. Guo, J. Liu, Y. Li, J. Caro, and A. Huang, “Post-synthetic modification of highly stable UiO-66-NH2 membranes on porous ceramic tubes with enhanced H2 separation,” *Microporous Mesoporous Mater.*, vol. 313, no. December 2020, p. 110823, 2021, doi: 10.1016/j.micromeso.2020.110823.

[37] Y. S. Lin, “Inorganic Membranes for Process Intensification: Challenges and Perspective,” *Ind. Eng. Chem. Res.*, vol. 58, no. 15, pp. 5787–5796, 2019, doi: 10.1021/acs.iecr.8b04539.

[38] S. P. Cardoso, I. S. Azenha, Z. Lin, I. Portugal, A. E. Rodrigues, and C. M. Silva, “Inorganic Membranes for Hydrogen Separation,” *Sep. Purif. Rev.*, vol. 47, no. 3, pp. 229–266, 2018, doi: 10.1080/15422119.2017.1383917.

[39] M. He *et al.*, “High hydrogen permeable ZIF-8 membranes on double modified substrates,” *Sep. Purif. Technol.*, vol. 275, no. June, 2021, doi: 10.1016/j.seppur.2021.119109.

[40] Z. Lai, “Development of ZIF-8 membranes: opportunities and challenges for commercial applications,” *Curr. Opin. Chem. Eng.*, vol. 20, pp. 78–85, 2018, doi: 10.1016/j.coche.2018.03.002.

[41] Y. Liu, X. Wang, Y. Zhang, Y. He, and X. Gu, “Scale-up of NaA zeolite membranes on α-Al2O3 hollow fibers by a secondary growth method with vacuum seeding,” *Chinese J. Chem. Eng.*, vol. 23, no. 7, pp. 1114–1122, 2015, doi: 10.1016/j.cjche.2015.04.006.

[42] L. S. M. Nazir, Y. F. Yeong, and T. L. Chew, “Methods and synthesis parameters affecting the formation of FAU type zeolite membrane and its separation performance: a review,” *J. Asian Ceram. Soc.*, vol. 8, no. 3, pp. 553–571, 2020, doi: 10.1080/21870764.2020.1769816.

[43] S. Friebe, B. Geppert, F. Steinbach, and J. Caro, “Metal-Organic Framework UiO-66

Layer: A Highly Oriented Membrane with Good Selectivity and Hydrogen Permeance," *ACS Appl. Mater. Interfaces*, vol. 9, no. 14, pp. 12878–12885, 2017, doi: 10.1021/acsami.7b02105.

[44] D. Shi, X. Yu, W. Fan, V. Wee, and D. Zhao, "Polycrystalline zeolite and metal-organic framework membranes for molecular separations," *Coord. Chem. Rev.*, vol. 437, p. 213794, 2021, doi: 10.1016/j.ccr.2021.213794.

[45] A. Farjoo, S. M. Kuznicki, and M. Sadrzadeh, "Hydrogen separation by natural zeolite composite membranes: Single and multicomponent gas transport," *Materials (Basel).*, vol. 10, no. 10, pp. 1–14, 2017, doi: 10.3390/ma10101159.

[46] S. Lee, J. Kim, J. Kim, and D. Lee, "Zeolitic Imidazolate Framework Membrane with Marked Thermochemical Stability for High-Temperature Catalytic Processes," *Chem. Mater.*, vol. 30, no. 2, pp. 447–455, 2018, doi: 10.1021/acs.chemmater.7b04409.

[47] Y. Li, G. Zhu, Y. Wang, Y. Chai, and C. Liu, "Preparation, mechanism and applications of oriented MFI zeolite membranes: A review," *Microporous Mesoporous Mater.*, vol. 312, no. August 2020, p. 110790, 2021, doi: 10.1016/j.micromeso.2020.110790.

[48] M. Malekmohammadi, S. Fatemi, M. Razavian, and A. Nouralishahi, "A comparative study on ZIF-8 synthesis in aqueous and methanolic solutions: Effect of temperature and ligand content," *Solid State Sci.*, vol. 91, no. January, pp. 108–112, 2019, doi: 10.1016/j.solidstatesciences.2019.03.022.

[49] N. A. B. Fauzan *et al.*, "Composite amine mixed matrix membranes for high-pressure CO 2 -CH 4 separation: Synthesis, characterization and performance evaluation: Composite Amine Mixed Matrix Membranes," *R. Soc. Open Sci.*, vol. 7, no. 9, 2020, doi: 10.1098/rsos.200795rsos200795.

[50] C. O. C. H. Separation, "Synthesis and Preparation of Asymmetric PSf / ZIF-8 Mixed Matrix Membrane for Jurnal Teknologi Full paper Synthesis and Preparation of Asymmetric PSf / ZIF-8 Mixed Matrix," vol. 9, no. August, pp. 8–12, 2014.

[51] H. Yin, T. Lee, J. Choi, and A. C. K. Yip, "On the zeolitic imidazolate framework-8

(ZIF-8) membrane for hydrogen separation from simulated biomass-derived syngas," *Microporous Mesoporous Mater.*, vol. 233, pp. 70–77, 2016, doi: 10.1016/j.micromeso.2015.10.033.

[52] G. Gundiah, M. Eswaramoorthy, S. Neeraj, S. Natarajan, and C. N. R. Rao, "Synthesis and characterization of submicron-sized mesoporous aluminosilicate spheres," *Proc. Indian Acad. Sci. Chem. Sci.*, vol. 113, no. 3, pp. 227–234, 2001, doi: 10.1007/BF02704072.

[53] C. Casado-Coterillo, "Mixed matrix membranes," *Membranes (Basel).*, vol. 9, no. 11, pp. 1–5, 2019, doi: 10.3390/membranes9110149.

[54] G. Clarizia, C. Algieri, and E. Drioli, "Filler-polymer combination: A route to modify gas transport properties of a polymeric membrane," *Polymer (Guildf).*, vol. 45, no. 16, pp. 5671–5681, 2004, doi: 10.1016/j.polymer.2004.06.001.

[55] T. W. Pechar *et al.*, "Fabrication and characterization of polyimide-zeolite L mixed matrix membranes for gas separations," *J. Memb. Sci.*, vol. 277, no. 1–2, pp. 195–202, 2006, doi: 10.1016/j.memsci.2005.10.029.

[56] P. Gorgojo, S. Uriel, C. Téllez, and J. Coronas, "Development of mixed matrix membranes based on zeolite Nu-6(2) for gas separation," *Microporous Mesoporous Mater.*, vol. 115, no. 1–2, pp. 85–92, 2008, doi: 10.1016/j.micromeso.2007.11.046.

[57] Z. Qiao, Z. Wang, C. Zhang, S. Yuan, Y. Zhu, and J. Wang, "PVAm–PIP/PS composite membrane with high performance for CO_2/N_2 separation," *AIChE J.*, vol. 59, no. 4, pp. 215–228, 2012, doi: 10.1002/aic.

[58] A. M. W. Hillock, S. J. Miller, and W. J. Koros, "Crosslinked mixed matrix membranes for the purification of natural gas: Effects of sieve surface modification," *J. Memb. Sci.*, vol. 314, no. 1–2, pp. 193–199, 2008, doi: 10.1016/j.memsci.2008.01.046.

[59] M. Rezakazemi, K. Shahidi, and T. Mohammadi, "Hydrogen separation and purification using crosslinkable PDMS/zeolite A nanoparticles mixed matrix membranes," *Int. J. Hydrogen Energy*, vol. 37, no. 19, pp. 14576–14589, 2012, doi:

10.1016/j.ijhydene.2012.06.104.

[60] C. I. Chaidou, G. Pantoleontos, D. E. Koutsonikolas, S. P. Kaldis, and G. P. Sakellaropoulos, “Gas Separation Properties of Polyimide-Zeolite Mixed Matrix Membranes,” *Sep. Sci. Technol.*, vol. 47, no. 7, pp. 950–962, 2012, doi: 10.1080/01496395.2011.645263.

[61] M. Hussain and A. König, “Mixed-Matrix Membrane for Gas Separation: Polydimethylsiloxane Filled with Zeolite,” *Chem. Eng. Technol.*, vol. 35, no. 3, pp. 561–569, 2012, doi: 10.1002/ceat.201100419.

[62] S. U. Azam, A. Hussain, S. Farrukh, T. Noor, and Y. Liu, “Enhancement in the selectivity of O2/N2 via ZIF-8/CA mixed-matrix membranes and the development of a thermodynamic model to predict the permeability of gases,” *Environ. Sci. Pollut. Res.*, vol. 27, no. 19, pp. 24413–24429, 2020, doi: 10.1007/s11356-020-08778-1.

[63] T. H. Bae, J. S. Lee, W. Qiu, W. J. Koros, C. W. Jones, and S. Nair, “A high-performance gas-separation membrane containing submicrometer-sized metal-organic framework crystals,” *Angew. Chemie - Int. Ed.*, vol. 49, no. 51, pp. 9863–9866, 2010, doi: 10.1002/anie.201006141.

[64] T. Yang, Y. Xiao, and T. S. Chung, “Poly-/metal-benzimidazole nano-composite membranes for hydrogen purification,” *Energy Environ. Sci.*, vol. 4, no. 10, pp. 4171–4180, 2011, doi: 10.1039/c1ee01324f.

[65] T. Li, Y. Pan, K. V. Peinemann, and Z. Lai, “Carbon dioxide selective mixed matrix composite membrane containing ZIF-7 nano-fillers,” *J. Memb. Sci.*, vol. 425–426, pp. 235–242, 2013, doi: 10.1016/j.memsci.2012.09.006.

[66] A. Ehsani and M. Pakizeh, “Synthesis, characterization and gas permeation study of ZIF-11/Pebax® 2533 mixed matrix membranes,” *J. Taiwan Inst. Chem. Eng.*, vol. 66, pp. 414–423, 2016, doi: 10.1016/j.jtice.2016.07.005.

[67] M. Amin *et al.*, “Conversion of Waste Biomass into Activated Carbon and Evaluation of Environmental Consequences Using Life Cycle Assessment,” pp. 1–12, 2022.

[68] Z. W. Dunbar and D. Chu, “Thin palladium membranes supported on microstructured nickel for purification of reformate gases,” *J. Power Sources*, vol. 217, pp. 47–53, 2012, doi: 10.1016/j.jpowsour.2012.05.044.

[69] Y. Li, X. Zhang, R. Yang, G. Li, and C. Hu, “The role of H3PO4 in the preparation of activated carbon from NaOH-treated rice husk residue,” *RSC Adv.*, vol. 5, no. 41, pp. 32626–32636, 2015, doi: 10.1039/c5ra04634c.

[70] R. A. Zerbonia, C. M. Brockmann, P. R. Peterson, and D. Housley, “Carbon bed fires and the use of carbon canisters for air emissions control on fixed-roof tanks,” *J. Air Waste Manag. Assoc.*, vol. 51, no. 12, pp. 1617–1627, 2001, doi: 10.1080/10473289.2001.10464393.

[71] O. Oginni, K. Singh, G. Oporto, B. Dawson-Andoh, L. McDonald, and E. Sabolsky, “Influence of one-step and two-step KOH activation on activated carbon characteristics,” *Bioresour. Technol. Reports*, vol. 7, no. June, p. 100266, 2019, doi: 10.1016/j.biteb.2019.100266.

[72] Y. Huang, E. Ma, and G. Zhao, “Thermal and structure analysis on reaction mechanisms during the preparation of activated carbon fibers by KOH activation from liquefied wood-based fibers,” *Ind. Crops Prod.*, vol. 69, pp. 447–455, 2015, doi: 10.1016/j.indcrop.2015.03.002.

[73] J. Xu, L. Chen, H. Qu, Y. Jiao, J. Xie, and G. Xing, “Preparation and characterization of activated carbon from reedy grass leaves by chemical activation with H 3 PO 4,” *Appl. Surf. Sci.*, vol. 320, pp. 674–680, Nov. 2014, doi: 10.1016/j.apsusc.2014.08.178.

[74] J. Bedia, M. Peñas-Garzón, A. Gómez-Avilés, J. J. Rodriguez, and C. Belver, “Review on Activated Carbons by Chemical Activation with FeCl3,” *C — J. Carbon Res.*, vol. 6, no. 2, p. 21, 2020, doi: 10.3390/c6020021.

[75] Z. Xu *et al.*, “Fabrication of cotton textile waste-based magnetic activated carbon using FeCl3 activation by the Box-Behnken design: optimization and characteristics,” *RSC Adv.*, vol. 8, no. 66, pp. 38081–38090, 2018, doi: 10.1039/c8ra06253f.

[76] Y. Gao, Q. Yue, B. Gao, and A. Li, “Insight into activated carbon from different kinds of chemical activating agents: A review,” *Sci. Total Environ.*, vol. 746, p. 141094, 2020, doi: 10.1016/j.scitotenv.2020.141094.

[77] Suhdi and S. C. Wang, “Fine activated carbon from rubber fruit shell prepared by using zncl2 and koh activation,” *Appl. Sci.*, vol. 11, no. 9, 2021, doi: 10.3390/app11093994.

[78] Y. Liu *et al.*, “Synthesis of Activated Carbon from Citric Acid Residue by Phosphoric Acid Activation for the Removal of Chemical Oxygen Demand from Sugar-Containing Wastewater,” *Environ. Eng. Sci.*, vol. 36, no. 6, pp. 656–666, 2019, doi: 10.1089/ees.2018.0506.

[79] Y. Shi, G. Liu, L. Wang, and H. Zhang, “Activated carbons derived from hydrothermal impregnation of sucrose with phosphoric acid: Remarkable adsorbents for sulfamethoxazole removal,” *RSC Adv.*, vol. 9, no. 31, pp. 17841–17851, 2019, doi: 10.1039/c9ra02610j.

[80] C. Saka, “BET, TG-DTG, FT-IR, SEM, iodine number analysis and preparation of activated carbon from acorn shell by chemical activation with ZnCl2,” *J. Anal. Appl. Pyrolysis*, vol. 95, pp. 21–24, 2012, doi: 10.1016/j.jaap.2011.12.020.

[81] G. Özsin, M. Kılıç, E. Apaydın-Varol, and A. E. Pütün, “Chemically activated carbon production from agricultural waste of chickpea and its application for heavy metal adsorption: equilibrium, kinetic, and thermodynamic studies,” *Appl. Water Sci.*, vol. 9, no. 3, 2019, doi: 10.1007/s13201-019-0942-8.

[82] E. M. Mistar, T. Alfatah, and M. D. Supardan, “Synthesis and characterization of activated carbon from Bambusa vulgaris striata using two-step KOH activation,” *J. Mater. Res. Technol.*, vol. 9, no. 3, pp. 6278–6286, 2020, doi: 10.1016/j.jmrt.2020.03.041.

[83] H. K. Yağmur and İ. Kaya, “Synthesis and characterization of magnetic ZnCl2-activated carbon produced from coconut shell for the adsorption of methylene blue,” *J. Mol. Struct.*, vol. 1232, 2021, doi: 10.1016/j.molstruc.2021.130071.

[84] W. Simanjuntak, S. Sembiring, P. Manurung, R. Situmeang, and I. M. Low,

"Characteristics of aluminosilicates prepared from rice husk silica and aluminum metal," *Ceram. Int.*, vol. 39, no. 8, pp. 9369–9375, 2013, doi: 10.1016/j.ceramint.2013.04.112.

[85] W. Aulia *et al.*, "Synthesis and Characterization of Zeolitic Imidazolate Framework-8 (ZIF-8)/Al2O3 Composite," *IPTEK J. Technol. Sci.*, vol. 31, no. 1, p. 18, 2020, doi: 10.12962/j20882033.v31i1.5511.

[86] X. Ma and D. Liu, "Zeolitic imidazolate framework membranes for light olefin/paraffin separation," *Crystals*, vol. 9, no. 1, pp. 1–26, 2019, doi: 10.3390/cryst9010014.

[87] F. Chen, S. Dong, Z. Wang, J. Xu, R. Xu, and J. Wang, "Preparation of mixed matrix composite membrane for hydrogen purification by incorporating ZIF-8 nanoparticles modified with tannic acid," *Int. J. Hydrogen Energy*, vol. 45, no. 12, pp. 7444–7454, 2020, doi: 10.1016/j.ijhydene.2019.04.050.

[88] L. Yu, M. S. Nobandegani, A. Holmgren, and J. Hedlund, "Highly permeable and selective tubular zeolite CHA membranes," *J. Memb. Sci.*, vol. 588, no. July, p. 117224, 2019, doi: 10.1016/j.memsci.2019.117224.

[89] Q. Song *et al.*, "Zeolitic imidazolate framework (ZIF-8) based polymer nanocomposite membranes for gas separation," *Energy Environ. Sci.*, vol. 5, no. 8, pp. 8359–8369, 2012, doi: 10.1039/c2ee21996d.

[90] M. He *et al.*, "High hydrogen permeable ZIF-8 membranes on double modified substrates," *Sep. Purif. Technol.*, vol. 275, no. May, 2021, doi: 10.1016/j.seppur.2021.119109.

[91] W. Li, S. A. S. C. Samarasinghe, and T. H. Bae, "Enhancing CO2/CH4 separation performance and mechanical strength of mixed-matrix membrane via combined use of graphene oxide and ZIF-8," *J. Ind. Eng. Chem.*, vol. 67, pp. 156–163, 2018, doi: 10.1016/j.jiec.2018.06.026.

[92] A. Julbe and M. Drobek, "Zeolite Membrane," *Encycl. Membr.*, pp. 2056–2057, 2016, doi: 10.1007/978-3-662-44324-8_605.

[93] B. Chen, Z. Yang, Y. Zhu, and Y. Xia, “Zeolitic imidazolate framework materials: Recent progress in synthesis and applications,” *J. Mater. Chem. A*, vol. 2, no. 40, pp. 16811–16831, 2014, doi: 10.1039/c4ta02984d.

[94] A. C. Yang, T. Y. Wang, C. A. Dai, and D. Y. Kang, “Incorporation of single-walled aluminosilicate nanotubes for the control of crystal size and porosity of zeolitic imidazolate framework-L,” *CrystEngComm*, vol. 18, no. 6, pp. 881–887, 2016, doi: 10.1039/c5ce02031j.

국문 초록

이 연구에서 ZIF 분리먹은 활성탄 및 알루미노실리케이트와 통합했다. 제조된 분리막은 메탄가스, 이산화탄소 가스 등의 가스 분리에 사용했다.

활성탄 제조를 위해 H_3PO_4 를 활성화제로 사용하여 풍부한 기공 구조로 만들었다. 조류에서 추출한 활성탄의 BET(Brunauer-Emmett-Teller) 표면적은 783 m^2/g 이다. 갈조류로부터 제조된 활성탄은 85%의 탄소 함량을 나타냈다. 알루미노실리케이트의 XRD 분석은 알루미노실리케이트가 구조적으로 결정질임을 보여준다. 알루미노실리케이트의 표면적은 943 m^2g^{-1} 로 측정되었다. 생성된 멤브레인의 SEM 이미지는 알루미노실리케이트의 통합이 계면 공극 형성을 향상시키고 형태의 기공 차단을 개선한다. 활성탄을 첨가하면 활성탄의 높은 표면적 때문에 멤브레인의 표면이 상대적으로 더 다공성인 성질을 나타낸다.

ZIF 분리막의 투과 결과는 상온에서 H_2 와 CO_2 의 투과값이 각각 3164.17, 156.11 (Barrer)인 것으로 나타났다. ZIF-AC-AS 분리막의 투과 결과는 상온에서 CH_4 와 CO_2 의 투과값이 각각 207.46, 232.23 (Barrer) 인 것으로 나타났다. 상온에서 100℃까지 온도가 상승함에 따라 CH_4 와 CO_2 의 투과도 값은 각각 146.86 과 203.58 Barrer 로 약간 감소하였다. 따라서, 이 연구는 ZIF 구조에서 활성탄과 알루미노실리케이트가 기체 투과성을 증가시킨다는 것을 보여주었다.

본 논문 작성자는 한국정부초청장학금(Global Korea Scholarship)을 지원받은 학생임.